

## Water Resources Research

### RESEARCH ARTICLE

10.1029/2017WR021985

#### Key Points:

- Bankfull Shields number is inversely related to bank sediment size
- Predictive relationships for bankfull geometry of sand-bed streams are adapted to consider bank sediment size
- Sand-bed deltas with distributary channel networks maintain smaller Shields numbers

#### Supporting Information:

- Supporting Information S1
- Data Set S1
- Data Set S2
- Data Set S3

#### Correspondence to:

T. Dong,  
td10@rice.edu

#### Citation:

Dong, T. Y., Nittrouer, J. A., Czapiga, M. J., Ma, H., McElroy, B., Il'icheva, E., et al. (2019). Roles of bank material in setting bankfull hydraulic geometry as informed by the Selenga River Delta, Russia. *Water Resources Research*, 55. <https://doi.org/10.1029/2017WR021985>

Received 1 OCT 2017

Accepted 28 APR 2018

© 2019. American Geophysical Union.  
All Rights Reserved.

# Roles of Bank Material in Setting Bankfull Hydraulic Geometry as Informed by the Selenga River Delta, Russia

Tian Y. Dong<sup>1</sup> , Jeffrey A. Nittrouer<sup>1</sup> , Matthew J. Czapiga<sup>2</sup>, Hongbo Ma<sup>1</sup> ,  
Brandon McElroy<sup>3</sup> , Elena Il'icheva<sup>4,5</sup>, Maksim Pavlov<sup>4</sup>, Sergey Chalov<sup>6</sup> , and Gary Parker<sup>2,7</sup> 

<sup>1</sup>Department of Earth, Environmental, and Planetary Science, Rice University, Houston, TX, USA, <sup>2</sup>Department of Civil and Environmental Engineering, University of Illinois at Urbana-Champaign, Urbana, IL, USA, <sup>3</sup>Department of Geology and Geophysics, University of Wyoming, Laramie, WY, USA, <sup>4</sup>Laboratory of Hydrology and Climatology, V.B. Sochava Institute of Geography, Siberian Branch Russian Academy of Science, Irkutsk, Russian Federation, <sup>5</sup>Department of Hydrology and Environmental Sciences, Irkutsk State University, Irkutsk, Russian Federation, <sup>6</sup>Faculty of Geography, M. V. Lomonosov Moscow State University, Moscow, Russian Federation, <sup>7</sup>Department of Geology, University of Illinois at Urbana-Champaign, Champaign, IL, USA

**Abstract** A semi-empirical bankfull Shields number relation as a function of slope, bed, and bank sediment grain size is obtained based on a field data set that includes the delta of the Selenga River, Russia, and other rivers from around the globe. The new Shields number relation is used in conjunction with continuity, flow resistance, and sediment transport equations to deduce predictive relations for bankfull width, depth, and slope of sand-bed rivers. In addition, hydraulic geometry relations are obtained specifically for the Selenga River delta. Key results of this study are as follows: (1) bankfull width is strongly dependent on water discharge and is directly related to bank sediment size; (2) bankfull shear velocity is weakly dependent on bed sediment size and is inversely related to bank sediment size; (3) sand-bed deltas with multiple distributary channels maintain smaller bankfull Shields numbers than is typical of alluvial rivers. This analysis is the first of its kind to include bank sediment size into a predictive bankfull Shields number relation to obtain relations for bankfull hydraulic geometry. The relations presented here can be utilized in morphodynamic models that explore how fluvial and deltaic systems respond to a range of imposed conditions, such as variable base level, sediment, and water supply.

## 1. Introduction

### 1.1. Bankfull Hydraulic Geometry

One of the central questions in the field of fluvial geomorphology is what framework best predicts the equilibrium bankfull hydraulic geometry of alluvial rivers given a set of catchment-scale parameters, such as water and sediment discharge. Reliable hydraulic geometry relations have practical engineering applications for the management and design of both natural and artificial river structures (Lane et al., 1959). Moreover, bankfull geometry relationships provide tools for geoscientists to predict the responses of channel morphology to variable base level, water, and sediment supply, all of which are critical properties predicted to vary with ongoing climate change (Foreman et al., 2012; Parker et al., 2008).

The bankfull condition of a river is defined by the water discharge at which the flow spills from the channel onto the adjacent floodplain and is often estimated to be equivalent to the 1.5–2 years recurrence flood (Leopold et al., 1964; Leopold & Maddock, 1953; Leopold & Wolman, 1957). Later studies have determined that the return period of bankfull events is variable between different river systems on a range from 1 to up to 32 years (Williams, 1978). For the bankfull condition, the channel is characterized by six core variables: bankfull depth ( $H_{bf}$ ), bankfull width ( $B_{bf}$ ), bankfull water discharge ( $Q_{bf}$ ), sediment supply at bankfull flow ( $Q_{tbf}$ ), bed sediment size ( $D_{bed}$ ), and bed slope ( $S$ ). Predictive relations for bankfull channel geometry are obtained in terms of these variables, either empirically determined via field measurements, or theoretically derived from mass and momentum balance of water and sediment discharge. In the former case, predictive equations are typically in the form of power law functions between  $H_{bf}$ ,  $B_{bf}$ ,  $S$ , and  $Q_{bf}$  e.g.,  $B_{bf} = a Q_{bf}^b$ , where  $a$  and  $b$  are a coefficient and an exponent that vary by up to 30% due to differences in river properties, including bed material size, form drag, vegetation type, and bank

strength (Andrews, 1984; Hey & Thorne, 1986; Lee & Julien, 2006; Leopold & Maddock, 1953; Simons & Albertson, 1960).

Theoretical approaches combine equations of flow continuity, resistance, sediment transport, and/or bankfull Shields number to obtain predictive relations for  $H_{bf}$ ,  $B_{bf}$ , and  $S$  (Millar, 2005; Parker et al., 2007; Wilkerson & Parker, 2011). Shields number ( $\tau^*$ ) scales the ratio of fluid force on a sediment particle to the weight of the particle (Shields, 1936):

$$\tau^* = \frac{\tau}{\rho R g D_{50}} \quad (1)$$

where  $\tau$  is bed shear stress,  $\rho$  is water density,  $R$  is sediment submerged specific gravity,  $g$  is gravitational acceleration, and  $D_{50}$  is median bed grain size. Assuming steady and uniform flow, momentum balance at the bankfull condition is reduced to  $\tau_{bf} = \rho g H_{bf} S$ , and combining this relation with equation (1) yields the following form of bankfull Shields number ( $\tau_{bf}^*$ ):

$$\tau_{bf}^* = \frac{H_{bf} S}{R D_{50}} \quad (2)$$

Bankfull Shields numbers of gravel bed rivers have often been found to be 1–1.4 times greater than the critical Shields number ( $\tau_c^*$ , indicates threshold of motion) based on field observations and theoretical analysis (Lane, 1955; Parker, 1978a, 1978b; Parker et al., 2007, Phillips & Jerolmack, 2016). It also has been suggested that rivers maintain a roughly constant bankfull Shields number for gravel bed ( $\tau_{bf}^* = 0.049$ ) and for sand-bed ( $\tau_{bf}^* = 1.86$ ) rivers (Parker, 2004; Parker et al., 2008). However, recent empirical evidence has shown that the bankfull Shields number is a variable depending on a series of parameters, such as the dimensionless bed material grain size ( $D^* = \frac{(Rg)^{1/3}}{\nu^{2/3}} D_{50}$  (Van Rijn, 1984), where  $\nu$  is the kinematic viscosity of water), channel slope, and sediment supply (Li et al., 2015, 2016; Pfeiffer et al., 2017; Trampus et al., 2014).

Interestingly, previous equations for a variable bankfull Shields number rely on in-channel characteristics including  $D_{50}$  and  $S$ , and do not include properties of the channel bank. However, in nature, the floodplain and channel are highly interconnected environments (Dietrich et al., 1999; Howard, 1992). For example, a river channel is most morphodynamically active at or above bankfull conditions, when sediment-laden water emerges from the channel and starts to spread sediment across the adjacent floodplain (Leopold et al., 1964). Moreover, Li et al. (2015, 2016) showed a surprising result: bankfull shear velocity ( $u_{bf}^* = \sqrt{g R D_{50} \tau_{bf}^*}$ , modified from equation (2)) and depth are nearly independent of bed material size. This study proposes to test the hypothesis that bankfull Shields number shows a dependence on channel bank properties, such as bank sediment grain size, by using robust field measurements of bank properties from the Selenga River delta, Russia. This system possesses a gravel-sand transition over a relatively short spatial scale and contains diverse bank morphologies and hydrodynamic flow conditions (i.e., normal flow to back-water conditions progressing downstream (Dong et al., 2016).

The objectives presented herein are to: (1) obtain bankfull hydraulic geometry and Shields number relations for the Selenga River delta, (2) generate a bankfull Shields number relation that considers properties of the channel banks, (3) apply this relation along with continuity, resistance, and sediment transport equations to obtain new predictive relations for  $H_{bf}$ ,  $B_{bf}$ , and  $S$  for sand-bed rivers under variable water discharge ( $Q_{bf}$ ), sand supply ( $Q_{tbf}$ ), bed sediment size ( $D_{bed}$ ), and bank properties, and (4) characterize how the three dependent variables  $H_{bf}$ ,  $B_{bf}$ , and  $S$  vary as functions of channel bank properties.

## 2. Background

### 2.1. Previous Hydraulic Geometry Studies That Included Channel Bank Characteristics

Hydraulic geometry relations that incorporate channel bank characteristics are mainly obtained theoretically using the maximum efficiency approach, which was later extended into the optimum theory (Eaton & Millar, 2017; Millar, 2005; Millar & Quick, 1993; Singh, 2003). These researches hypothesize that equilibrium river geometry adjusts to an optimum configuration that maximizes sediment transport efficiency ( $\eta$ ), where  $\eta = \frac{Q_{tbf}}{Q_{bf} S}$  (modified from Millar, 2005; Eaton and Millar, 2017). For this approach, equations of fluid flow and sediment transport are iteratively solved to obtain hydraulic geometry relations that maximizes  $\eta$ , while maintaining stable channel banks. These studies utilize the framework of bank stability analysis as the

additional equation instead of the bankfull Shields number relation; these are based on geotechnical criteria for slope failure (Darby & Thorne 1996; Huang, 1983; Millar & Quick, 1993; Simon & Collison, 2002; Simon et al., 1991, 2000).

Subsequent studies have simplified and/or extended the bank failure analysis to sand-bed and gravel-bed channels with both cohesive and noncohesive bank materials, while accounting for the effects of vegetation/root cohesion (Eaton & Giles, 2009; Eaton & Millar, 2004; Millar, 2005). As these studies have shown, the bank morphology of an alluvial river is controlled by a range of factors, such as pore pressure and cohesion, and determination of the role for each of these factors based on field data is challenging due to measurement uncertainties and spatial variability (Darby & Thorne, 1996; Eaton & Millar, 2004; Simon & Collison, 2002). Hence, in this study, for simplicity, characteristic bank material size (here corresponding to median bank sediment size  $D_{50, bank}$ ) is used as a first-order characterization of bank properties.

## 2.2. Selenga River Delta

The Selenga River delta is located at the southeastern margin of Lake Baikal, an intracontinental rift basin, which has been tectonically active for the last ~35 million years (Figure 1a) (Krivonogov & Safonova, 2016). As indicated by seismic imaging, Cenozoic sediment thickness is 7.5–10 km in the southern Baikal Basin just offshore of the Selenga Delta, and 4–4.5 km in the northern Baikal Basin (Figure 1b) (Hutchinson et al., 1992; Logatchev, 1974; Krivonogov & Safonova, 2016).

The Selenga River enters the lake approximately normal to the rift axis and contributes about half of the total annual sediment and water delivered to Lake Baikal (Chalov et al., 2016; Coleman, 1998). Covering ~600 km<sup>2</sup>, the modern Selenga River delta is one of the largest lacustrine deltas in the world. It contains

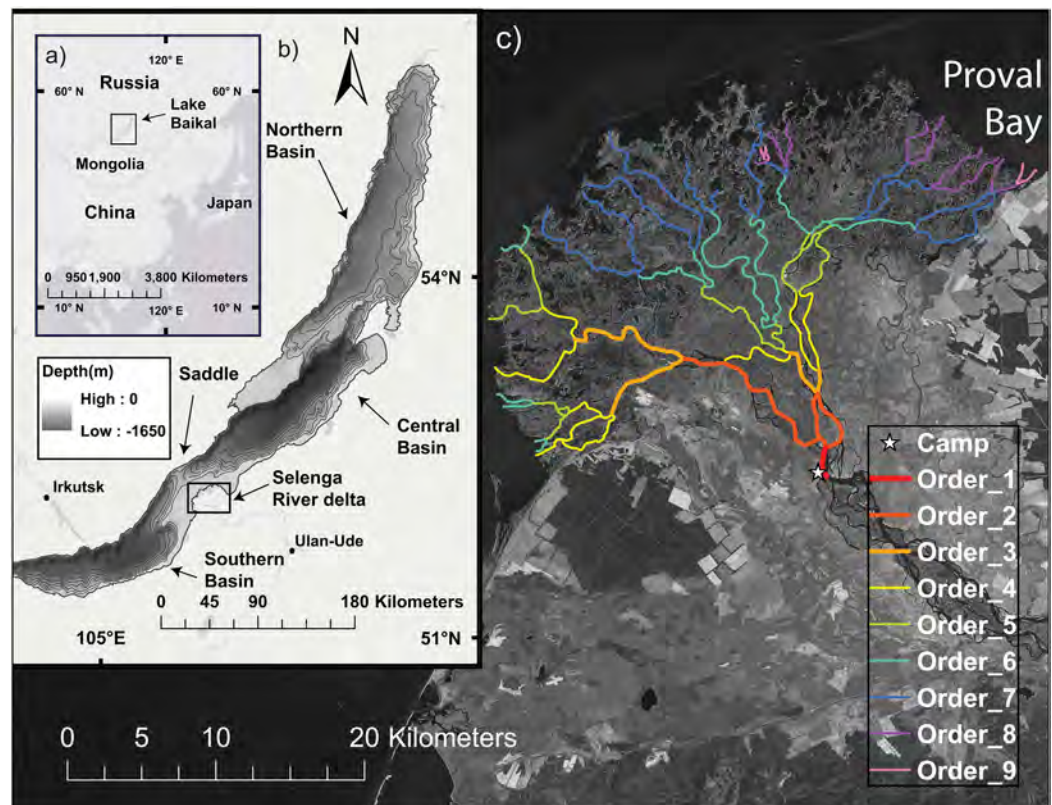


**Figure 1.** (a) Lake Baikal is located in southeastern Siberia, Russia. (b) Bathymetric map of the lake. With depth over 1.6 km and extending near 700 km in length, Lake Baikal is the largest lake in the world by volume. The Selenga River delta (highlighted in the black box) is the largest water and sediment source to the lake. It has created a bathymetric saddle that separates the Southern and Central Basins of Lake Baikal. (c) Satellite image of the delta. Bankfull shear velocity, channel geometry, vegetation, and bank morphology vary substantially within the nine orders of the bifurcating channel network (see text for detail). Colored image is available online.

three active lobes with multiple distributary channels that receive varying amounts of water and sediment (Coleman, 1998; Gyninova & Korsunov, 2006; Il'icheva, 2008; Il'icheva et al., 2014; Scholz et al., 1998). A previous study has classified the orders of the distributary channels using topological method of Hack (1957) and Dong et al., (2016). Selenga River mainstream is classified as a first-order channel. The delta system then bifurcates downstream into two second-order channels, and so on, with a total of nine channel orders identified (Figure 1c).

Within the deltaplain, distributary channels exhibit normal flow conditions in the upstream reaches, and transition to backwater influenced downstream reaches (Dong et al., 2016). Previous research has documented that over a relatively short distance ( $\sim 35$  km), channel bed sediment size fines downstream by three orders of magnitude, from coarse gravel at the apex to mud and fine sand near the delta margin (Dong et al., 2016; Il'icheva et al., 2014). Concomitantly, bank morphology changes from forested subaerial banklines to subaqueous levees with floating vegetation (Figures 2b–2e). Sediment transport capacity also decreases downstream as water is partitioned through the bifurcating channel network. This effect, combined with episodic tectonically driven subsidence, prevents the gravel-sand transition from reaching the delta fringe (Dong et al., 2016).

Deltas and their distributary channels are traditionally characterized as net-depositional landscapes, i.e., systems in a state of disequilibrium (Galloway, 1975; Gilbert, 1885). Here equilibrium/grade is defined as a stable river profile, such that the water and sediment supply and base level vary around a stable value for a long period of time (Blom et al., 2016; Lane, 1955; Mackin, 1948). Most of the distributary channels, specifically, first-order to fifth-order channels of the Selenga River delta are upstream of the influence of nonuniform flow and thus maintain normal flow conditions. In addition, the gravel-sand transitions within the normal flow portion of the delta network are arrested in position due to long-term episodic tectonic subsidence driven by the Baikal Rift (Cui & Parker, 1998; Dong et al., 2016; Parker & Cui, 1998). Based on these lines of evidence, it is inferred that much of the Selenga River delta can be considered to be at or near grade. Moreover, results from physical experiments indicate that a delta residing on the margin of a deep receiving basin achieves equilibrium for constant base level (i.e., “forced grade,” Muto et al., 2016); as is the case for the Selenga River delta, which resides in a deep basin with consistent water elevation as a shelf-edge deltaic system (Coleman, 1998). Thus, with its spatially varying channel types, bank morphologies and flow conditions, the Selenga River delta offers a rare opportunity to explore controls on equilibrium hydraulic channel geometry for multiple styles of rivers, including braided (gravel bed), wandering (mixed gravel-sand bed), and meandering (sand-bed), transitioning from a normal flow reach to a backwater reach, all in one geographic setting.

### 3. Methods

#### 3.1. Bank Characteristics

Channel bankline surveys were conducted in three major distributary channels of the Selenga River delta (number of survey transects,  $n = 34$ ; Figure 2a) during a flood discharge condition ( $Q = \sim 2,000$  m<sup>3</sup>/s) in summer 2016. Channels were selected based on the amount of water and sediment discharge received within their respective lobes (Il'icheva, 2008; Il'icheva et al., 2014). At each transect, a geomorphic survey was conducted at both banks following the method of Kellerhals et al. (1976) and Hey and Thorne (1986) (see details in Table 1). Four sediment samples were collected at each survey transect, at  $\sim 20$  cm depth and near the water surface for both eroding and accreting banks. The downstream distance between each survey transect ranged between 2.5 and 4 km.

It is important to point out that some of the data collected on the Selenga River delta have been specifically excluded from the analysis. That is, data were excluded where the river was interpreted to be eroding into a terrace. This is because the sediment size in terrace material may be unrelated to current formative processes in the channel. These terraces are found to exist within first-order to third-order distributary channels (Figure 2a). Also, two survey transects were omitted within a newly avulsed distributary channel, because this channel is likely to be far from morphodynamic equilibrium (Figure 2a).

#### 3.2. Bed and Bank Sediment

Grain-size distributions of bank sediments were determined using a laser diffraction analyzer (Malvern Mastersizer 2000) for muddy samples, and a dynamic image analyzer (Retsch Technology CAMSIZER) for

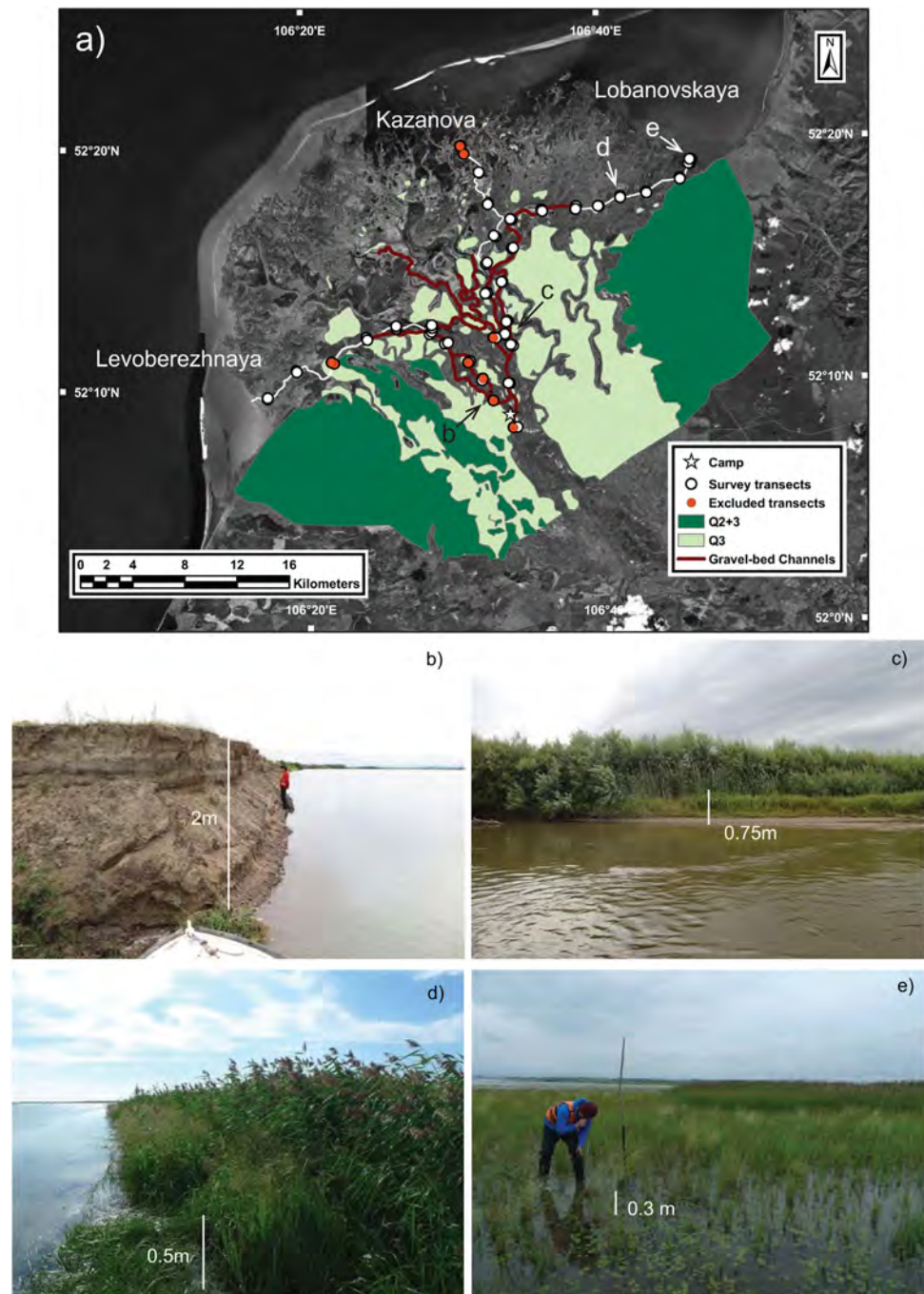


**Figure 2.** (a) Map showing locations of survey transects from summer 2016, indicated by white circles, where channel geometry, bed sediment size, bankfull velocity, and discharge data are available. Additionally, mixed sand-gravel channels of the modern Selenga Delta wander through relict terraces ( $Q_2$  and  $Q_3$  are Quaternary age deposits, by which  $Q_2$  is older than  $Q_3$ ; map was made by Kulchitsky (1964)). Data from transects within the terrace region, indicated by the orange circle, are omitted from the data analysis. (b–e) Photographs of the channel bank, illustrating downstream change (from (b–e)) in-channel morphology, a pattern that is particularly characterized by downstream decrease in bank and vegetation height.

samples that contain coarse sand and gravel. The percentage of organic matter (% O.M.) was measured using a standard loss on ignition (LOI) method (Heiri et al., 2001). Rouse number ( $Z_R$ ) is computed for each grain-size class (number of bins = 36) of bank grain-size distributions (GSD), such that  $Z_R = \frac{w_s}{\kappa u_{bf}^*}$ , where  $u_{bf}^*$  is bankfull shear velocity (as calculated in section 3.4),  $w_s$  is particle settling velocity; calculated using the

**Table 1**  
Channel Bank Survey Scheme

Category	Procedures
Bank Type	<i>Exposed</i> —Nonvegetated vertical to subvertical bank face <i>Covered</i> —Vegetated bank face <i>Bar</i> —Point bar (vegetated and nonvegetated) <i>Submerged</i> —Subaqueous banks
Bank State <sup>a</sup>	<i>Erosional</i> <i>Depositional</i> <i>Vegetation aggradation</i> —Can be erosional or depositional <i>Stable</i> —Neither erosional and depositional
Bank Elevation	Measured from top of the bank to the water surface. Absolute elevation measured using RTK GPS at top of the bank
Bank Slope	<i>Subaerial bank slope</i> —Measured by total station <i>Subaqueous slope</i> —Measured with tape measure and graded rod, combined with bathymetry data of channel cross-section
Vegetation Type	<i>Type</i> —Grass, shrub, tree, floating vegetation, aquatic vegetation <i>Tree count</i> —Number of trees in a controlled area, typically $\sim 40 \text{ m}^2$ <i>Root depth</i> —Included root depth of active grass-type and estimation of the tree root depth determined via augering
Sediment Samples	At least two samples per bank, one at $\sim 20 \text{ cm}$ depth, and another at water surface level

<sup>a</sup>Grazing and slump blocks status is noted.

method of Dietrich (1982), and  $\kappa = 0.41$  is von Kármán's constant. Grain-size classes that move purely as bedload are removed from each GSD using a  $Z_R > 2.5$  cutoff. A characteristic bank sediment grain-size distribution (GSD) is then computed for each transect by averaging all GSDs (without bedload) from both banks. A single value of  $D_{50, \text{bank}}$  was obtained from this GSD for the following analysis (Figure 3a). Bed sediment data were collected in 2013 and 2014 at the same survey locations (Dong et al., 2016) (Figures 2b and 3b).

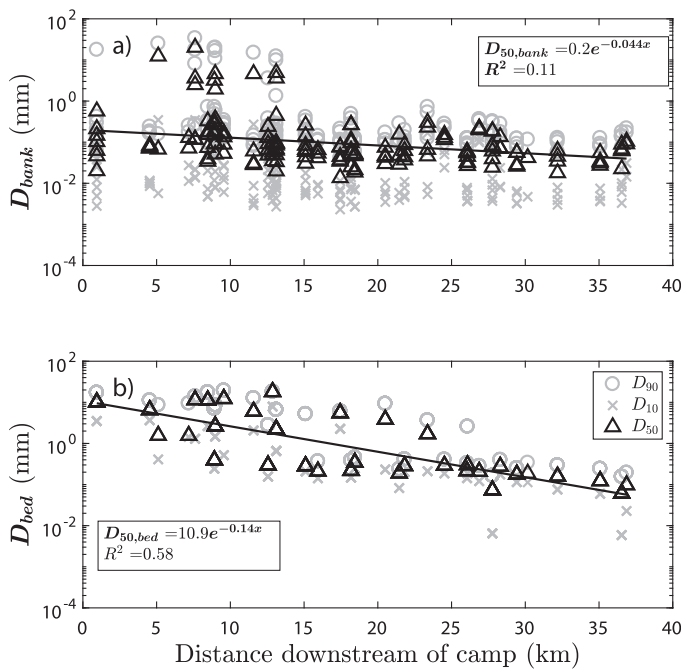


**Figure 3.** (a) Grain-size data from channel bank sediment collected in three main distributary channels of the Selenga Delta. Sediment size varies by three orders of magnitude from coarse gravel ( $\sim 24 \text{ mm}$ ) on upstream point bars to muddy subaqueous bank sediment at the delta margin. (b) Grain-size data of channel bed sediment. Sediment size varies by three orders of magnitude over the 35 km length of the delta topset.

### 3.3. Bankfull Channel Geometry

A LOWRANCE HDS-7 Gen. 2 fish finder was used to measure water depth at each survey site. Bankfull width was measured using both bathymetry and satellite imagery. Also, by combining measured bathymetry and bank elevation data (see section 3.4), bankfull cross-sectional channel area ( $A_{bf}$ ) was calculated by integrating water depth with respect to bankfull width. Bankfull depth was then calculated as  $H_{bf} = \frac{A_{bf}}{B_{bf}}$ .

### 3.4. Bankfull Shear Velocity and Shields Number

Bank elevation was measured at each survey location using a Trimble Real Time Kinematic (RTK) GPS. Water surface elevation was measured using a total station referenced to the known bank elevation measured by the RTK GPS (Figure 4). Since regions of the three surveyed channels are near normal flow condition and the backwater effects diminish at flood stage, bankfull shear velocity ( $u_{bf}^*$ ) is calculated by the depth-slope product for each transect:  $u_{bf}^* = \sqrt{gH_{bf}S}$ . To validate the computed shear velocity, velocity profiles were measured using a Russian-made propeller-driven velocimeter at near bankfull condition ( $Q = \sim 2,000 \text{ m}^3/\text{s}$ ; number of transects with velocity profiles,  $n = 28$ ). Each transect contains one velocity profile at the thalweg, with 4–7 measurement points. Flow velocity was measured at 10 cm intervals from the channel bottom to  $\sim 30 \text{ cm}$  above the bed, and at 0.5 m intervals until the propeller reached the water surface. Assuming hydraulically rough flow, shear velocity ( $u^*$ ) and roughness height ( $k_s$ ) were computed from the velocity profiles based on the Law of the Wall (e.g., Garcia, 2008). The measured

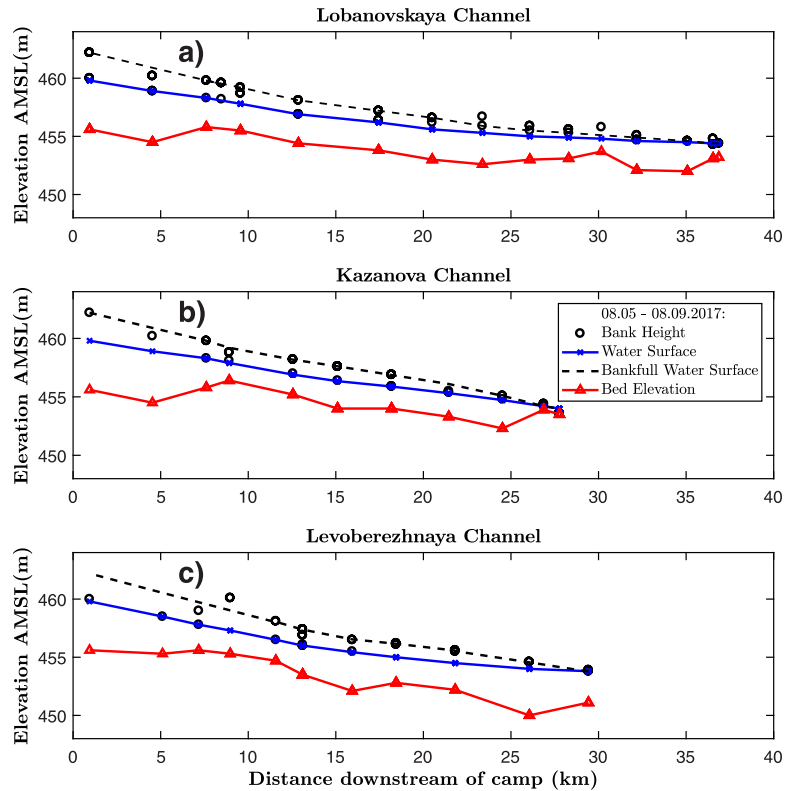


**Figure 4.** (a–c) Channel bank height, mean bed profile, flood (measured between 5 and 8 August 2016) and bankfull water surface elevation (interpreted based on bank elevation) for each of the three surveyed distributary channels of the Selenga River delta. Elevations are reported as meters above mean sea level.

shear velocity compares somewhat well with the computed bankfull shear velocity (Figure 5a). The low  $R^2$  in that figure is expected because measured shear velocity is a representation of local stress condition at flood discharge, while the calculated shear velocity is a measure of reach-averaged bankfull stress. Regardless, all data are within a factor of two. Bankfull Shields number is computed by its normal flow definition for each survey transect (equation (2)) and we explore the relationship between this value and bank properties below.

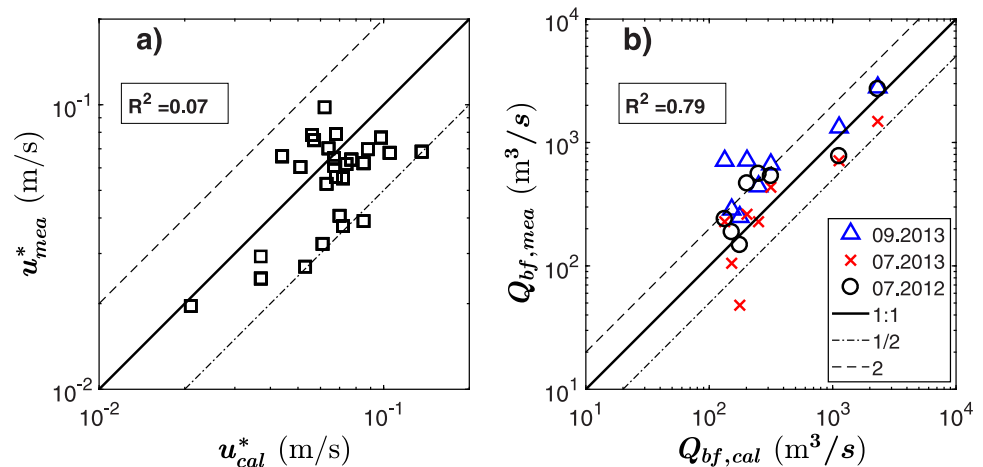


**Figure 5.** (a) Calculated bankfull shear velocity (b) and water discharge versus measured values under flood and bankfull conditions of the Selenga River delta ( $Q_w > 2,500 \text{ m}^3/\text{s}$ ). Dashed lines 2:1/1:2 show that most calculations fall within a factor of two of the measurements.

### 3.5. Bankfull Discharge

Since flow velocities were measured during a flood discharge ( $Q = \sim 2,000 \text{ m}^3/\text{s}$ ) and not a bankfull discharge, the Manning-Strickler resistance relation was used to compute water discharge for the bankfull condition ( $Q > 2,500 \text{ m}^3/\text{s}$ ) (e.g., Parker, 2004):

$$C_f^{-0.5} = \alpha \left( \frac{H_{bf}}{k_s} \right)^{1/6}, \quad (3a)$$

$$Q_{bf} = C_f^{-0.5} u_{bf}^* A_{bf}, \quad (3b)$$

where  $\alpha$  is a coefficient equal to 8.1 (Parker et al., 1991),  $C_f$  is the friction coefficient, and  $k_s$  is a roughness height extracted from the measured velocity profiles. For the survey transects without velocity profiles, roughness height is calculated as  $k_s = 3D_{90}$  (Van Rijn, 1984). Calculated bankfull water discharge compared reasonably well to measured bankfull events of the Selenga River delta ( $R^2 = 0.79$ , Figure 5b) (Chalov et al., 2016; Il'icheva et al., 2015).  $B_{bf}$ ,  $H_{bf}$ , and  $Q_{bf}$  are then normalized by bed material size and bankfull water discharge (Bray, 1982; Parker et al., 2003, 2007):

$$\tilde{B} = \frac{g^{1/5} B_{bf}}{Q_{bf}^{2/5}}, \quad (4a)$$

$$\tilde{H} = \frac{g^{1/5} H_{bf}}{Q_{bf}^{2/5}}, \quad (4b)$$

$$\hat{Q} = \frac{Q_{bf}}{\sqrt{gD_{50}} D_{50}^2}. \quad (4c)$$

### 3.6. Relating Bank Material to Bankfull Shields Number

To produce a new relationship for bankfull Shields number that includes a dependence on bank sediment size, we propose an empirical relationship between the primary variables ( $S$ ,  $H_{bf}$ ,  $D_{bed}$ ,  $D_{bank}$ ) that represents an extension of Trampush et al. (2014) (equation (5) therein):

$$\log S = \alpha_0 + \alpha_1 \log H_{bf} + \alpha_2 \log D_{bed} + \alpha_3 \log D_{bank}. \quad (5)$$

Rearranging equation (5) to obtain a relation for bankfull flow depth, it is found that:

$$\log H_{bf} = -\frac{\alpha_0}{\alpha_1} + \frac{1}{\alpha_1} \log S - \frac{\alpha_2}{\alpha_1} \log D_{bed} - \frac{\alpha_3}{\alpha_1} \log D_{bank}. \quad (6)$$

Substituting equation (6) into the definition for bankfull Shields number (equation (2)), yields:

$$\log \tau_{bf}^* = -\frac{\alpha_0}{\alpha_1} - \log R + \left( \frac{1}{\alpha_1} + 1 \right) \log S - \left( \frac{\alpha_2}{\alpha_1} + 1 \right) \log D_{bed} - \frac{\alpha_3}{\alpha_1} \log D_{bank}. \quad (7)$$

Equation (7) is further reduced in terms of dimensionless bed and bank grain sizes via  $D^* = \frac{(Rg)^{1/3}}{v^{2/3}} D_{50}$  to obtain (Van Rijn, 1984):

$$\log \tau_{bf}^* = \gamma_0 + \gamma_1 \log S + \gamma_2 \log D_{bed}^* + \gamma_3 \log D_{bank}^*, \quad (8)$$

where  $\gamma_0 = -\frac{\alpha_0}{\alpha_1} - \log R + \frac{2}{3} \left( \frac{\alpha_2}{\alpha_1} + \frac{\alpha_3}{\alpha_1} + 1 \right) \log \frac{\sqrt{Rg}}{v}$ ,  $\gamma_1 = \left( \frac{1}{\alpha_1} + 1 \right)$ ,  $\gamma_2 = -\left( \frac{\alpha_2}{\alpha_1} + 1 \right)$ , and  $\gamma_3 = \frac{\alpha_3}{\alpha_1}$ .

Equation (8) provide a semi-empirical relationship between bankfull Shields number and, among other variables, bank sediment grain size. To determine the values of the coefficients  $\alpha_0$ ,  $\alpha_1$ ,  $\alpha_2$ , and  $\alpha_3$ , multiple linear regression is applied to a data set of alluvial rivers and deltas that includes measurements of bank sediment size, and values of  $\gamma_0$ ,  $\gamma_1$ ,  $\gamma_2$ , and  $\gamma_3$  are obtained by rearranging the regression results shown in the above derivation. It is important to realize that this data set does not include data from Trampush et al. (2014) and Li et al. (2015, 2016), as neither of these include information on bank material. Our data set ( $n = 204$ ) includes measurements for  $H_{bf}$ ,  $D_{50}$ ,  $S$ , and bank material  $D_{bank}$ . Data were collected from the Selenga River delta (Figure 3b, mixed sand-bed and gravel bed, this study), gravel rivers from United Kingdom (Hey & Thorne, 1986), the middle Fly River (sand-bed) from Papua New Guinea (Dietrich et al., 1999), the Siret River (gravel bed to sand-bed) from Hungary (Ichim & Radoane, 1990), and the Llano River (mixed bedrock to

alluvial) from central Texas (Heitmuller & Hudson, 2009). Slopes of these rivers range from  $2.0 \times 10^{-5}$  to  $2.2 \times 10^{-2}$ , median bed material sizes range from 0.03 to 176 mm, median bank material sizes range from 0.005 to 6.2 mm, and bankfull flow depth ranges from 0.62 to 16.1 m.

### 3.7. Major Axis Regression

Measurement errors and uncertainties are inherently imbedded in the primary field variables ( $S$ ,  $H_{bfr}$ ,  $D_{bedr}$ , and  $D_{bank}$ ). To account for errors in both dependent and independent variables in the regression analysis, major axis (MA) regression is used (Czapiga et al., in revision; Markovsky & Van Huffel, 2007):

$$(X+E)B = Y+F, \quad (9)$$

where  $X$  is the matrix of independent variables and  $Y$  is the dependent variable. Here  $E$  and  $F$  are error matrices for  $X$  and  $Y$ , respectively, and  $B$  (equivalent to the previously introduced terms  $a_0$ ,  $a_1$ ,  $a_2$ , and  $a_3$ ) is the solution that minimizes  $E$  and  $F$ . For MA regression, residuals are minimized in the direction orthogonal to the model  $\hat{Y}$  ( $\hat{Y}$  in the case of equations (5) and (8) defines a four-dimensional hyperplane), instead of orthogonal to the direction of  $X$  in ordinary least square regression. MA regression is typically solved using singular value decomposition (Golub & Van Loan, 1980). More details about the formulation can be found in Van Huffel (1989) and Markovskya and Van Huffel (2007).

### 3.8. Akaike Information Criterion

To compare the relative predictive quality between our relation for bankfull Shields number including bank material size against previous models obtained via different regression techniques (Li et al., 2015), the Akaike Information Criterion (AIC) is used (Akaike, 1974). For linear least square regressions, AIC is expressed as (Banks & Joyner, 2017):

$$AIC = n \ln \left( \frac{RSS}{n} \right) + 2K, \quad (10)$$

Here  $n$  is the number of observations,  $RSS$  is the residual sum of the squares, equal to  $\sum_{i=1}^n (\log y_i - \log \hat{y}_i)^2$ . For the case of equations (5) and (8),  $y$  is the observed value,  $\hat{y}$  is the predicted value, and  $K$  is the number of independent variables, which includes the intercept and residual (for equations (5) and (8),  $K = 5$ ). Note that the AIC method does not test the null hypothesis, instead, it provides a measurement of how close are predicted distributions obtained via applying the same data set to different models to the "true" distribution. More details of the AIC method can be found in Burnham and Anderson (2004) and Burnham et al. (2011). Here we compare three models, including MA regression models with and without the variable  $D_{bank}$ , and the ordinary least square regression model from Li et al. (2016), all applied to our data set. In general, a lower AIC value indicates greater predictive quality (i.e., smaller distance to the "true" distribution), and this is measured by  $\Delta AIC = AIC_{\min} - AIC$  (Akaike, 1974; Banks & Joyner, 2017; Burnham & Anderson, 2004). Models having  $\Delta AIC \leq 2$  have substantial support, those in which  $4 \leq \Delta AIC \leq 7$  have considerably less support, and models having  $\Delta AIC > 10$  have essentially no support (Burnham & Anderson, 2004).

## 4. Results

### 4.1. Hydraulic Geometry of the Selenga River Delta

Following conventional methods (e.g., Leopold & Maddock, 1953), we determine power law relations between measured slope, bankfull depth, and width of the Selenga River delta channels and bankfull water discharge using ordinary least square (OLS) regression (Figures 6a–6c):

$$B_{bf} = 20.3 Q_{bf}^{0.335 \pm 0.098}, \quad (11a)$$

$$H_{bf} = 0.257 Q_{bf}^{0.384 \pm 0.067}, \quad (11b)$$

$$S = 3.11 \times 10^{-5} Q_{bf}^{0.309 \pm 0.091}. \quad (11c)$$

Similar relations are obtained for the dimensionless parameters (equations (4a)–(4c)) using OLS regression (Figures 6d–6f):

$$\tilde{B} = 38.1 \hat{Q}^{-0.0241 \pm 0.022}, \quad (12a)$$

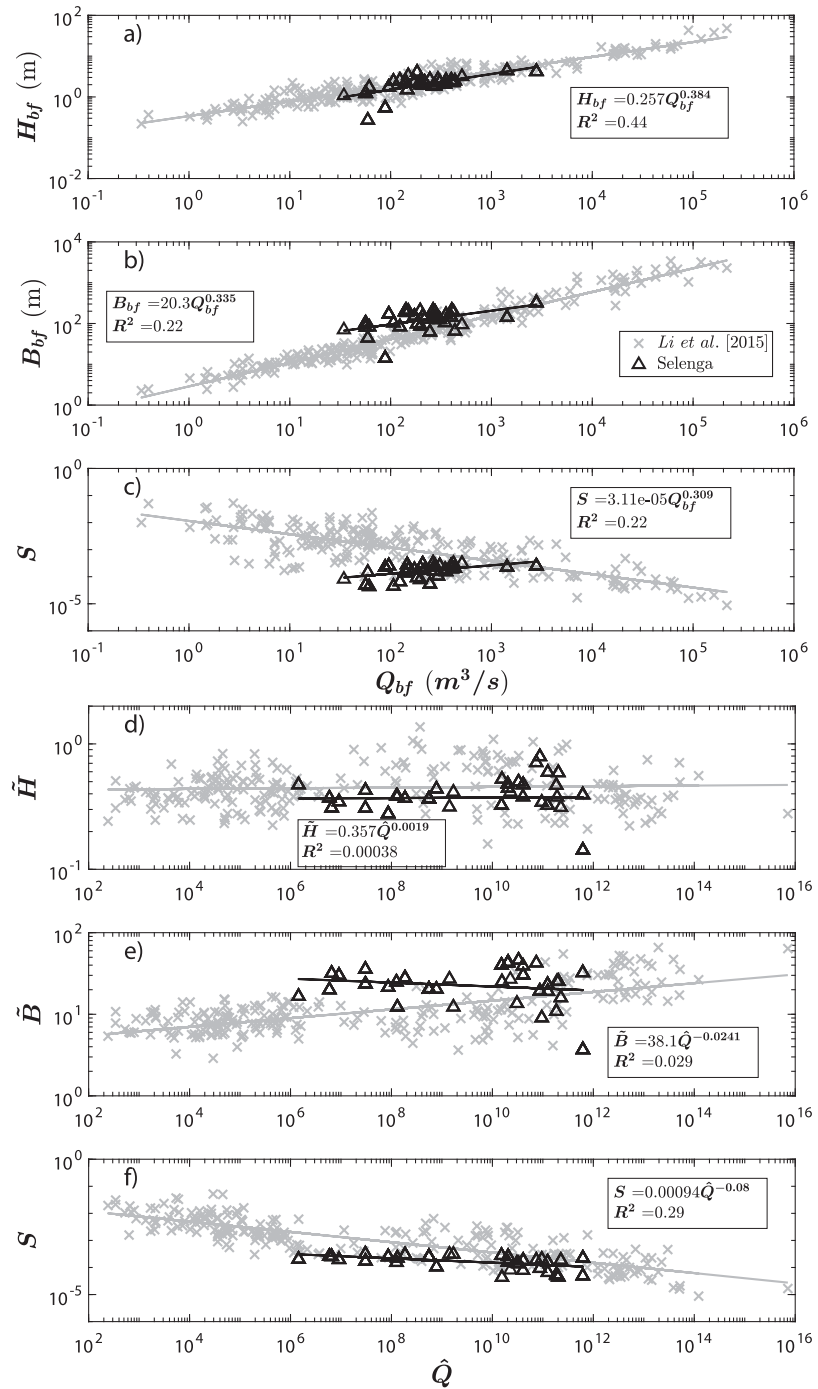


**Figure 6.** (a–c) Bankfull depth, width, and slope, and (d–f) their dimensionless values versus bankfull water discharge of the Selenga River delta. Results are superimposed over the data set of alluvial rivers from Li et al. (2015).

$$\tilde{H} = 0.357\hat{Q}^{0.0019 \pm 0.015}, \quad (12b)$$

$$S = 9.40 \times 10^{-4} \hat{Q}^{-0.0795 \pm 0.020}. \quad (12c)$$

For the above relations and the ones in subsequent sections, the uncertainties in the exponents were computed at the 95% confidence interval. In general, the exponent values from equations (11a) to (11c) and (12a) to (12c) are within the range of results from previous studies (see Table 2 for details) (Li et al., 2015; Parker et al., 2007; Wilkerson & Parker, 2011); in particular, bankfull depth and width increase with

**Table 2**  
Exponents of Flood Discharge, Sand Supply, Bed, and Bank Sediment Size in Predictive Relations for Bankfull Width, Depth, and Slope From Various Studies

	$B_{bf}$	$H_{bf}$	$S$
Constant	$Q_{bf}^{0.0} Q_{tbf}^{1.0} D_{bed}^{-1.5}$	$Q_{bf}^{1.0} Q_{tbf}^{-1.0} D_{bed}^{1.0}$	$Q_{bf}^{-1.0} Q_{tbf}^{1.0} D_{bed}^{0.0}$
This study (Selenga)	$Q_{bf}^{0.335}$	$Q_{bf}^{0.384}$	$Q_{bf}^{0.309}$
This study (Global)	$Q_{bf}^{0.69} Q_{tbf}^{0.31} D_{bed}^{0.14} D_{bank}^{0.33}$	$Q_{bf}^{0.36} Q_{tbf}^{-0.36} D_{bed}^{-0.24} D_{bank}^{-0.25}$	$Q_{bf}^{-0.75} Q_{tbf}^{0.75} D_{bed}^{0.68} D_{bank}^{0.14}$
Hey and Thorne (1986)	$Q_{bf}^{0.50}$	$Q_{bf}^{0.37} D_{50}^{-0.11}$	$Q_{bf}^{-0.31} D_{50}^{0.71}$
Millar (2005)	$Q_{bf}^{0.50} D_{50}^{-0.25}$	$Q_{bf}^{0.37} D_{50}^{0.075}$	$Q_{bf}^{-0.33} D_{50}^{0.825}$
Lee and Julien (2006)	$Q_{bf}^{0.426} D_{50}^{-0.002}$	$Q_{bf}^{0.336} D_{50}^{0.025}$	$Q_{bf}^{-0.346} D_{50}^{0.955}$
Parker et al. (2007)	$Q_{bf}^{0.467} D_{50}^{-0.167}$	$Q_{bf}^{0.400} D_{50}^{0.000}$	$Q_{bf}^{-0.344} D_{50}^{0.860}$
Wilkerson and Parker (2011)	$Q_{bf}^{0.669} D_{50}^{0.0685}$	$Q_{bf}^{0.276} D_{50}^{-0.155}$	$Q_{bf}^{-0.394} D_{50}^{0.691}$
Li et al. (2015, 2016)	$Q_{bf}^{0.57} Q_{tbf}^{0.43} D_{50}^{0.34}$	$Q_{bf}^{0.45} Q_{tbf}^{-0.45} D_{50}^{-0.38}$	$Q_{bf}^{-0.80} Q_{tbf}^{0.80} D_{50}^{0.76}$

increasing water discharge (Parker et al., 2007). As shown in Figures (6b) and (6e), the exponents of the bankfull width relations determined from the Selenga Delta data is within the lower range of values found in previous research (equations (11a) and (12a); Table 2).

#### 4.2. Bankfull Shields Numbers of the Selenga River Delta

Bankfull Shields numbers of the Selenga River delta were computed for each survey transect and compared to both measured slope ( $S$ ) and dimensionless bed sediment grain size ( $D_{bed}^*$ ). Shields number decreases with increasing  $D_{bed}^*$ , and increases with increasing slope in each grain-size class (Figures 7a and 7b), these patterns are consistent with results from previous studies (Dade & Friend, 1998; Li et al., 2015; Parker et al., 2007; Trampus et al., 2014; Wilkerson & Parker, 2011). Furthermore, bankfull Shields number varies by

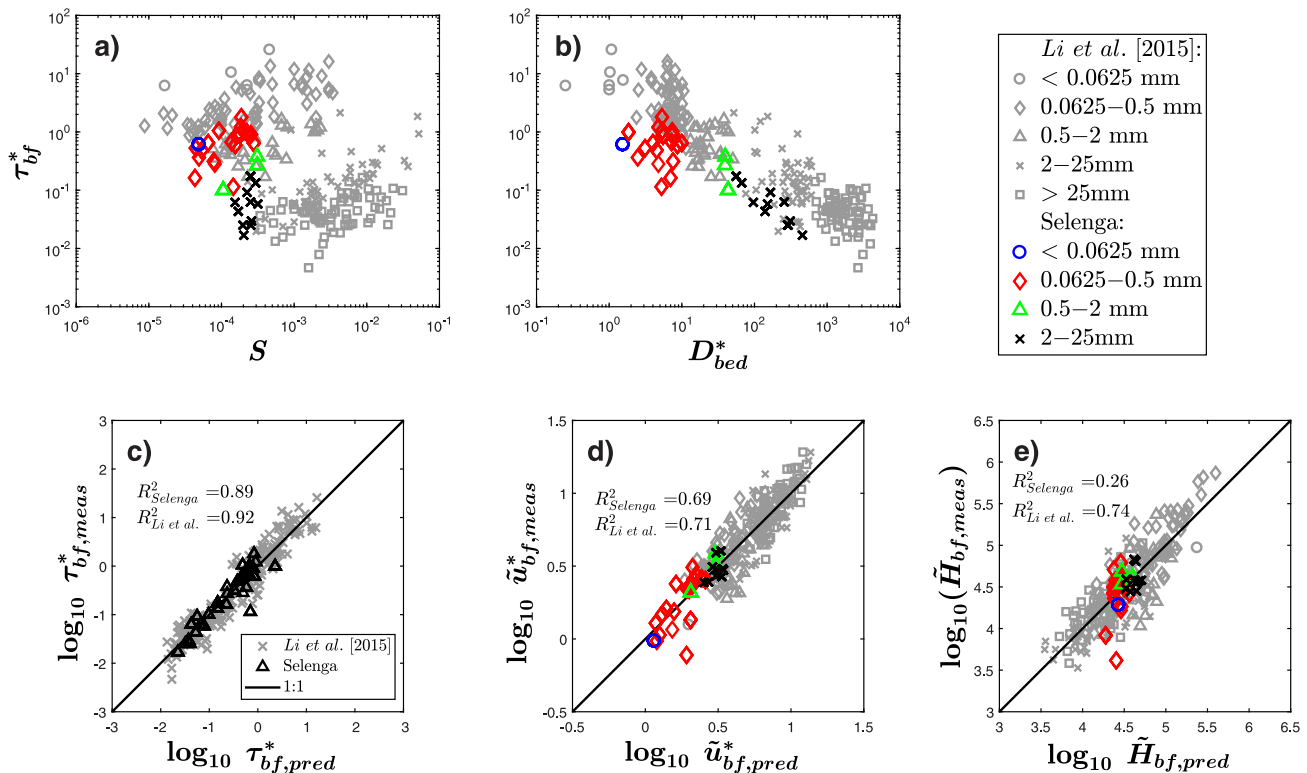


**Figure 7.** (a and b) Bankfull Shields number versus bed slope and dimensionless bed sediment size of the Selenga River delta, superimposed over the values from the data set of Li et al. (2015). (c and e) The predictive relations for bankfull Shields number, dimensionless shear velocity, and depth as functions of bed slope and grain size (see equations (13a)–(13c)).

nearly an order of magnitude within  $\sim 35$  km of channel network of the Selenga Delta (Figure 8e), because bed sediment size, slope, and bankfull depth all decrease downstream due to bifurcation (Figures 3b and 8a–8d) (Dong et al., 2016).

Following the method of Li et al. (2016), ordinary least square (OLS) multiple linear regression is conducted between  $\log \tau_{bf}^*$  and  $[\log S, \log D_{bed}^*]$  using data collected in the Selenga River delta. Although there are superior methods, OLS is used to compare to previous studies (Li et al., 2015), and yields (Figures 7c–7e):

$$\tau_{bf}^* = 1936 S^{0.742 \pm 0.144} D_{bed}^{*-0.824 \pm 0.047}, \quad (13a)$$

$$\tilde{u}_{bf}^* = 44 S^{0.371 \pm 0.072} D_{bed}^{*0.0879 \pm 0.024}, \quad (13b)$$

$$\tilde{H}_{bf} = 1936 S^{-0.258 \pm 0.144} D_{bed}^{*0.176 \pm 0.047}, \quad (13c)$$

where  $\tilde{u}_{bf}^*$  and  $\tilde{H}_{bf}$  are dimensionless bankfull shear velocity and depth, defined independently of grain size as  $\tilde{u}_{bf}^* = \frac{u_{*bf}}{(Rg\nu)^{1/3}}$  and  $\tilde{H}_{bf} = \frac{H_{bf}g^{1/3}}{(R\nu)^{2/3}}$  (Li et al., 2015). Exponents of equations (13a)–(13c) are compared with values from Li et al. (2016) in Figures 7c–7e. To first order, the exponent values obtained for the Selenga channels are different to those of Li et al. (2016). Specifically,  $\tau_{bf}^*$  is proportional to  $D_{bed}^{*-0.824}$  (exponent equal to  $-0.951$  for Li et al. (2016)). However, in both cases, bankfull shear velocity is nearly independent of bed grain size (exponent equal to  $0.0879$ ). Bankfull depth is less dependent on slope (exponent equal to  $-0.566$

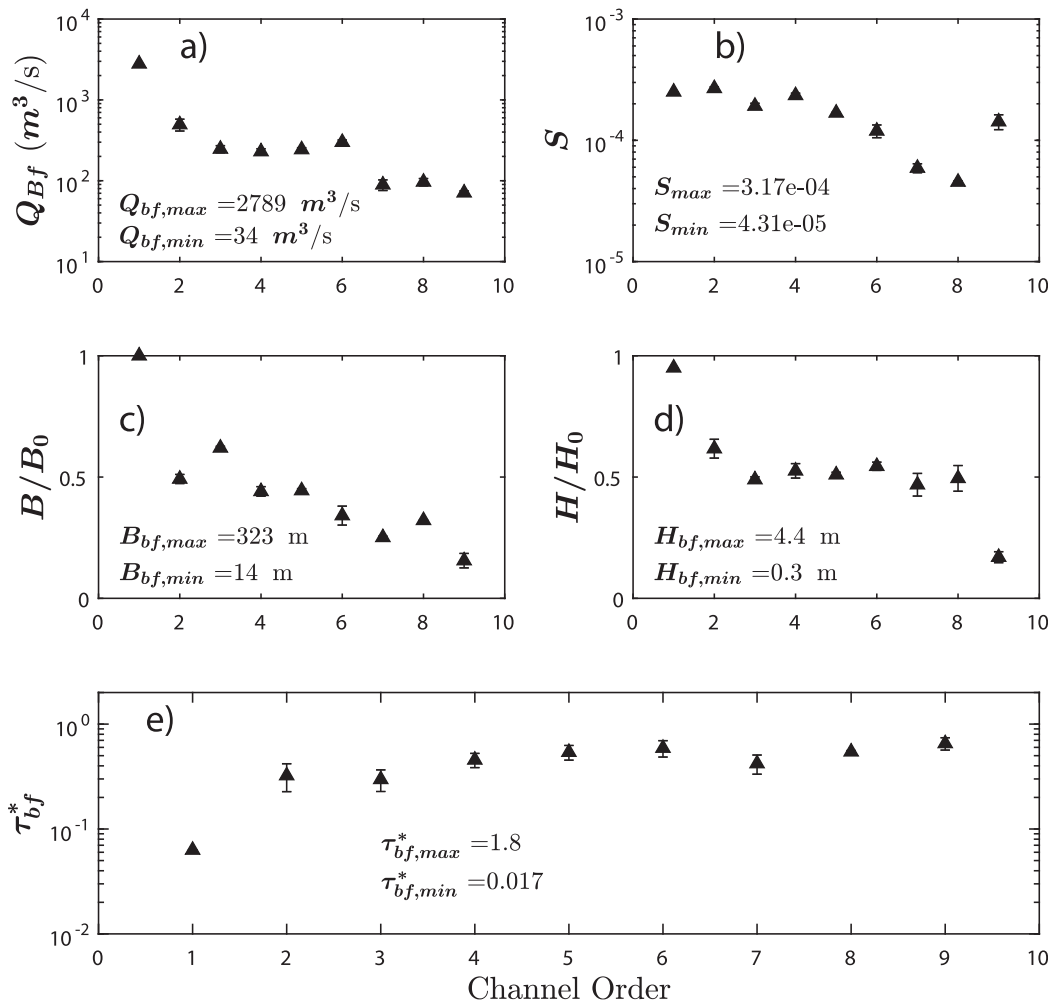


**Figure 8.** (a) Calculated bankfull water discharge versus channel order (modified from Dong et al., 2016). (b) Slope versus channel order. (c) Normalized channel width ( $B/B_0$ ,  $B_0$  = width of first-order channel) versus channel order. (d) Normalized channel depth ( $H/H_0$ ,  $H_0$  = width of first-order channel) versus channel order. (e) Bankfull Shields number versus channel order. Bars on data points represent standard error of the mean (SEM).

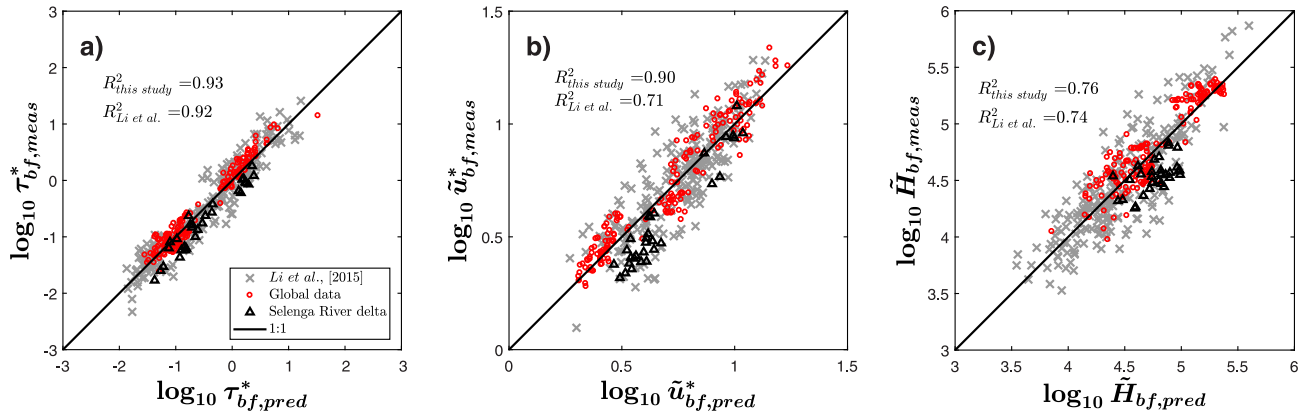


**Figure 9.** (a–c) Predictive relations for bankfull Shields number, dimensionless shear velocity and depth as functions of bed slope, bed grain size, and bank grain size (see equations (14a)–(14c)). These data are superimposed onto a similar data set from Li et al. (2015, 2016), who did not consider bank grain size in their study.

in Li et al., 2016), whereas the exponent value for slope is larger for the Selenga Delta (0.217 in Li et al., 2016).

### 4.3. A New Relation for Bankfull Shields Number

Here we apply major axis (MA) regression of primary variables ( $S$ ,  $H_{bf}$ ,  $D_{bed}$ ,  $D_{bank}$ ) to a data set of alluvial rivers and deltas, including the Selenga Delta, to obtain a semi-empirical relationship between bankfull Shields number and bank sediment size in the form of equation (8) (see MATLAB code in supporting information, Figure 9a, and Table 3). The result is as follows:

$$\tau_{bf}^* = 932.9 S^{0.517 \pm 0.036} D_{bed}^{-0.907 \pm 0.028} D_{bank}^{-0.184 \pm 0.073}. \quad (14a)$$

Applying equation (14a) to the normal flow definition of bankfull Shields number (equation (2)) yields the following relations for dimensionless shear velocity and depth (Figures 9b and 9c):

$$\tilde{u}_{bf}^* = 30.5 S^{0.259 \pm 0.018} D_{bed}^{0.0468 \pm 0.014} D_{bank}^{-0.0920 \pm 0.037}, \quad (14b)$$

$$\tilde{H}_{bf} = 932.9 S^{-0.483 \pm 0.036} D_{bed}^{0.0935 \pm 0.028} D_{bank}^{-0.184 \pm 0.073}. \quad (14c)$$

Bankfull Shields number is seen to increase with increasing slope and decreasing bed and bank sediment size (equation (14a)). Bankfull shear velocity increases with increasing slope, bed sediment size, and decreasing bank sediment size (equation (14b)). Bankfull depth increases with decreasing slope, decreasing bank sediment size, and increasing bed sediment size (equation (14c)). Compared to previous studies, bankfull depth and shear velocity are weakly dependent on bed material grain size (see details in Table 3) (Li et al., 2016; Trampush et al., 2014). Part of the difference may be attributed to the difference in regression method; previous studies did not consider error in the dependent variable ( $S$  or  $H_{bf}$ ).

### 4.4. Predictive Quality of Different Bankfull Shields Number Models

The Akaike Information Criterion (AIC) is calculated (equation (10)) for MA regression with  $D_{bank}$ , MA regression without  $D_{bank}$  and OLS regression from Li et al. (2016) (see details in Table 4). The resulting AIC values

**Table 3**  
Values of Exponents on Slope, Dimensionless Bed, and Bank Sediment Size for Relations of Bankfull Shields Number, Dimensionless Shear Velocity and Depth From Various Studies

	$\tau_{bf}^*$	$\tilde{u}_{bf}^*$	$\tilde{H}_{bf}$
This study <sup>a</sup>	$932.9 S^{0.517} D_{bed}^{-0.907} D_{bank}^{-0.184}$	$30.5 S^{0.259} D_{bed}^{0.0468} D_{bank}^{-0.0920}$	$929.3 S^{-0.483} D_{bed}^{0.0935} D_{bank}^{-0.184}$
Li et al. (2016) <sup>a</sup>	$502 S^{0.434} D_{bed}^{-0.951}$	$22.4 S^{0.217} D_{bed}^{0.0245}$	$502 S^{-0.566} D_{bed}^{0.049}$
Trampush et al. (2014) <sup>a,b</sup>	$17.4 S^{0.08} D_{bed}^{-0.77}$	$4.17 S^{0.04} D_{bed}^{0.115}$	$17.4 S^{-0.92} D_{bed}^{0.23}$

<sup>a</sup>Rearranged into power law form. <sup>b</sup>Rearranged into the form of  $S$  and  $D_{bed}^*$ .

**Table 4**  
Akaike Information Criterion (AIC) for Different Regression Models

Method	Model <sup>a</sup>	<i>n</i>	<i>K</i>	AIC	ΔAIC <sup>+</sup>	<i>R</i> <sup>2</sup>	RMSE
MA	$\tau_{bf}^* = 932.9 S^{0.517} D_{bed}^{*-0.907} D_{bank}^{*-0.184}$	204	5	-698.7	0	0.93	0.176
MA	$\tau_{bf}^* = 691.2 S^{0.483} D_{bed}^{*-0.901}$	204	4	-673.1	25.6	0.92	0.188
OLS	$\tau_{bf}^* = 502 S^{0.434} D_{bed}^{*-0.951}$	204	4	-602.4	96.3	0.89	0.224
MA	$\tilde{u}_{bf}^* = 30.5 S^{0.259} D_{bed}^{*0.0468} D_{bank}^{*-0.092}$	204	5	-981.5	0	0.90	0.0882
MA	$\tilde{u}_{bf}^* = 26.3 S^{0.241} D_{bed}^{*0.0496}$	204	4	-955.9	25.6	0.88	0.0942
OLS	$\tilde{u}_{bf}^* = 22.4 S^{0.217} D_{bed}^{*0.0245}$	204	4	-885.1	96.4	0.83	0.112
MA	$\tilde{H}_{bf} = 932.9 S^{-0.483} D_{bed}^{*0.0935} D_{bank}^{*-0.184}$	204	5	-698.7	0	0.76	0.176
MA	$\tilde{H}_{bf} = 691.2 S^{-0.518} D_{bed}^{*0.099}$	204	4	-673.1	25.6	0.73	0.188
OLS	$\tilde{H}_{bf} = 502 S^{-0.566} D_{bed}^{*0.049}$	204	4	-602.4	96.3	0.62	0.224

<sup>a</sup>Rearranged into power law form. <sup>+</sup>ΔAIC = AIC<sub>min</sub> - AIC.

(Table 4) indicate that models of bankfull Shields number, shear velocity, and depth via MA regressions with  $D_{bank}$  have relatively greater prediction qualities than models via MA regression without  $D_{bank}$  and OLS regression from Li et al. (2016) (i.e., smaller AIC value). Moreover, in term of absolute predictive power, the models with  $D_{bank}$  has the highest coefficient of determination ( $R^2$ ) and lowest root mean squared error (RMSE) (Figure 9 and Table 4).

#### 4.5. General Closure Model for Bankfull Hydraulic Geometry of Sand-Bed Stream

Predictive relations for parameters associated with bankfull geometry,  $H_{bfr}$ ,  $B_{bfr}$ ,  $S$  under a given water discharge, sediment supply, bed, and bank grain size are derived by rearranging the new relation for bankfull Shields number (equation (14a)) subject to equations of water and sediment continuity, sediment transport, and flow resistance. The relations for water and sediment continuity are:

$$Q_{bf} = U_{bf} H_{bf} B_{bf}, \quad (15a)$$

$$Q_{tbf} = q_t B_{bf}, \quad (15b)$$

where  $Q_{tbf}$  is the total sediment discharge at bankfull, and  $q_t$  is the volumetric sediment transport rate per unit width. The dimensionless Chezy resistance is defined using an empirical relation to  $S$  (Li et al., 2015; Parker, 2004):

$$CZ = \frac{U_{bf}}{U_{bf}^*} = \alpha_R S^{-n_R}, \quad \alpha_R = 2.53, \quad n_R = 0.19. \quad (16)$$

In the case of sand-bed streams, the Engelund and Hansen (1967) total bed material load relation is appropriate (Ma et al., 2017):

$$q_t = \alpha_{EH} CZ^2 \sqrt{RgD_{bed}} D_{bed} \tau_{*bf}^{2.5}, \quad \alpha_{EH} = 0.05. \quad (17)$$

We use equation (14a) to specifically assess the impact of  $D_{bank}$  on  $B_{bfr}$ ,  $H_{bfr}$  and  $S$ , and to study the effect of bank material size on bankfull Shields number:

$$\tau_{*bf}^* = \beta S^m D_{bed}^{*n_1} D_{bank}^{*n_2},$$

$$\beta = 932.9, \quad m = 0.517, \quad n_1 = -0.907, \quad n_2 = -0.184. \quad (18)$$

Combining and reducing the above relations (equations (15a–18)), the following predictive relations for bankfull width, depth, and slope of sand-bed streams, which are analogous to those of Li et al. (2016) but specifically consider channel bank sediment size, are obtained:

$$\frac{B_{bf}}{D_{bed}} = \frac{1}{\sqrt{RgD_{bed}} D_{bed}^2 \alpha_{EH} \alpha_R^2 \beta^{2.5} D_{bed}^{2.5n_1} D_{bank}^{2.5n_2}}$$

$$\times \left[ \frac{R}{\alpha_{EH} \alpha_R \beta D_{bed}^{*n_1} D_{bank}^{*n_2}} \right]^{-(2.5m-2n_R)/(1+m-n_R)} \left( \frac{Q_{tbf}}{Q_{bf}} \right)^{-(2.5m-2n_R)/(1+m-n_R)} Q_{tbf}, \quad (19a)$$

$$\frac{H_{bf}}{D_{bed}} = \alpha_{EH} \alpha_R \beta^2 D_{bed}^{*2n_1} D_{bank}^{*2n_2}$$

$$\times \left[ \frac{R}{\alpha_{EH} \alpha_R \beta D_{bed}^{*n_1} D_{bank}^{*n_2}} \right]^{(2m-n_R)/(1+m-n_R)} \left( \frac{Q_{tbf}}{Q_{bf}} \right)^{(2m-n_R)/(1+m-n_R)} \frac{Q_{bf}}{Q_{tbf}}, \quad (19b)$$

$$S = \left[ \frac{R}{\alpha_{EH} \alpha_R \beta D_{bed}^{*n_1} D_{bank}^{*n_2}} \right]^{1/(1+m-n_R)} \left( \frac{Q_{tbf}}{Q_{bf}} \right)^{1/(1+m-n_R)}. \quad (19c)$$

The exponents for bankfull water discharge, sand supply, bed, and bank sediment size from equations (19a) to (19c) are reported and compared to the case of constant Shields number, as well as the forms in Li et al. (2016) in Table 2. More specifically, the exponents of the independent variables for equations (19a)–(19c) are given explicitly below:

$$B_{bf} \sim Q_{bf}^{0.69} Q_{tbf}^{0.31} D_{bed}^{0.14} D_{bank}^{0.33}, \quad (20a)$$

$$H_{bf} \sim Q_{bf}^{0.36} Q_{tbf}^{-0.36} D_{bed}^{-0.24} D_{bank}^{-0.25}, \quad (20b)$$

$$S \sim Q_{bf}^{-0.75} Q_{tbf}^{0.75} D_{bed}^{0.68} D_{bank}^{0.14}. \quad (20c)$$

In equations (20a)–(20c), bankfull width increases with increasing flood discharge, sand supply, bed sediment size, and bank sediment size (equation (20a)). Bankfull depth increases with increasing flood discharge, and decreasing sand supply, bed sediment size, and bank sediment size (equation (20b)). Slope increases with decreasing flood discharge, and increasing sand supply, bed sediment size, and bank sediment size (equation (20c)). We emphasize that such results explicitly including the effect of bank material on sand-bed hydraulic geometry have not been reported elsewhere.

## 5. Discussions

### 5.1. Bankfull Hydraulic Geometry and Shields Number Relations in a Distributary Network

Notable differences in the hydraulic geometry relations between the Selenga River delta (delta with distributary network) and other rivers (formed via tributary network) are apparent in the relationships between bed slope and bankfull water discharge and (Figure 6c), and the relationships between dimensionless channel width and bankfull water discharge (Figure 6e). In the Selenga Delta channels, slope increases with bankfull water discharge (positive exponent), which contradicts observations from non-deltaic alluvial rivers. A potential explanation for this discrepancy is that in the Selenga distributary channels, water discharge decreases downstream due to channel bifurcation (Figure 8a), and commensurately slope also declines downstream as the water surface of the channels approach the base level of Lake Baikal (i.e., asymptotic profile characteristic of backwater flow, Figures 4 and 8b). As a result, slope and water discharge are positively related, unlike typical nondeltaic alluvial rivers where slope and discharge are commonly inversely related when compared across different river systems. Moreover, the variation in slope likely arises due to a combination of downstream bed material fining, base level effect, and channel bifurcation.

To explain relationships between the dimensionless variables (equations (12a)–(12c)), it is important to first note that  $Q_{bf}$ ,  $H_{bf}$ , and  $B_{bf}$  all decrease downstream as a function of channel bifurcation order (Figures 8a, 8c, and 8d). Furthermore,  $Q_{bf}$  is normalized by bed material size (equation (4c)), which fines downstream by three orders of magnitude ( $D_{50, max} = 18$  mm,  $D_{50, min} = 0.063$  mm). As a result, dimensionless bankfull water discharge increases downstream by nearly five orders of magnitude ( $\hat{Q}_{min} = 1.44 \times 10^6$ ,  $\hat{Q}_{max} = 6.20 \times 10^{11}$ ). Meanwhile, spatial variability of bankfull width and depth remains the same after normalization (equations (4a) and (4b)), and slope decreases downstream by an order of magnitude (Figure 8b). Thus, slope, and normalized bankfull width and depth have very weak dependencies on dimensionless bankfull water discharge (shown by the exponent values of equations (12a)–(12c)). In addition,  $H_{bf}$ ,  $B_{bf}$ ,  $S$ , and  $Q_{bf}$  also contain measurement and calculation errors; specifically, the RTK GPS and single-beam sonar has  $\sim$ cm-scale measurement errors for altitude and water depth, respectively.

The bankfull Shields numbers for coarse sand and pebble gravel reaches in the Selenga River delta fall within the lower range of alluvial rivers, whereas Shields numbers for the medium and fine sand-bed channels are below the range of many alluvial rivers (Figures 7a and 7b). This is maybe because the medium and fine sand-bed alluvial rivers from the data set of Li et al. (2015) possess larger depth-slope product ( $H_{bf}S$ ) compared to the Selenga River delta. The sand-bed reaches with lower Shields number in the Selenga River delta are close to the delta-lake boundary where water surface slope decreases as they approach the base level of Lake Baikal (Figures 4a–4c and 8b). Meanwhile, flow depth in this region remains relatively constant (Figure 8d). Here adjustment of channel geometry due to partitioning of water discharge via bifurcation occurs mainly as a downstream reduction of channel width (Figure 8c). Therefore, the Selenga River delta has a smaller Shields number in its sand-bed reaches compared to other fluvial counterparts (Figures 7a and 7b).

### 5.2. Roles of Bank Material

In the proposed relationships (equations (20a)–(20c)), bankfull width is strongly dependent on water discharge and bank sediment size, such that  $B_{bf} \sim Q_{bf}^{0.69} D_{bank}^{0.33}$ . Although the result is empirical, the role of bank sediment size in this case can be interpreted as follows: as bank sediment size fines, cohesion increases, and bank erosion is reduced due to increased bank shear strength, the armoring effect of slump blocks and the interaction of fine-grained sediment and plant roots (Parker et al., 2011). The direct impact of bank sediment grain size can be characterized in terms of friction angle based on research of the threshold of sediment motion for channel bed material (Buffington et al., 1992; Kirchner et al., 1990; Wiberg & Smith, 1987). Typically, sediments with fine size and heterogeneous grain-size distribution have greater friction angle. For gravel bed rivers, assuming banks and bed are made of similar material, bank strength is characterized by a ratio between the friction angles of bed and bank materials (Millar, 2005). Previous model found that channel width decreases with increasing bank strength; in agreement with the finding of this study (equation (20a)) (Millar, 2005). In natural rivers, there usually is also a cohesive layer of fine sediments and vegetation capping a lower layer of coarser bank material. In this case, sediment cohesion comes into the picture of bank strength through Mohr-Coulomb failure analysis for saturated soil, by which channel bank strength increases with resistance force (e.g., Darby & Thorne, 1996; Eaton, 2006; Eaton & Giles, 2009; Simon et al., 2000, 1991). Additionally, root systems of vegetation are treated as a type of cohesion ( $c$ ), based on empirical studies, such that  $c_t = c + c_r$ ; where  $c_t$  is total cohesion and  $c_r$  is cohesion by roots (e.g., Wu et al., 1979; Zhang et al., 2010). Meanwhile, empirical data show that clay content increases soil cohesion (e.g., Aberle, 2004; Dafalla, 2013). Thus, vegetation and cohesive material increase bank strength and allow the bank height to increase.

Blocks of this cohesive upper bank layer may fail due to excess pore pressure after extended periods of rainfall, reduction of confining pressure during the falling stage of a flood, and fluvial undercutting during bankfull flow (Darby & Thorne, 1996; Eke et al., 2014; Millar & Quick, 1993; Parker et al., 2011). Upon failure, slump blocks deposit at the toe of the channel bank and thus protect the bank from river flow. Over time, cohesive blocks decay (erode), and vanish due to surface erosion and sediment entrainment (Gabet, 1998; Micheli & Kirchner, 2002). Bank erosion resumes until slump block failure subsequently occurs (Simon et al., 1999).

The dependence of flow depth on bank sediment size is revealed as an inverse relationship ( $H_{bf} \sim D_{bank}^{-0.25}$ , equation (20b)). Assuming steady and uniform flow, if a river channel widens as bank sediment size increases then the flow depth should decrease so as to maintain continuity. As a result, width-depth ratio is directly related to bank sediment size by a power law relation:  $\frac{B_{bf}}{H_{bf}} = 22.5 D_{bank}^{0.28}$  (Figure 10a). The data scattering around the power law model implies that there are maybe other bank characteristics affecting the width-depth ratio. In consideration of the bankfull shear velocity relation,  $u_{bf}^* = \sqrt{g H_{bf} S}$ , as bank sediment fines,  $u_{bf}^*$  is expected to increase due to increasing depth. Interestingly, increasing bank sediment relates to increasing slope in term of equation (20c),  $S \sim D_{bank}^{0.14}$ . Typically, slope decreases, and width-depth ratio increases downstream in alluvial rivers. Therefore, downstream fining of bank material is expected, as is illustrated for three rivers (in the case of the Selenga River, an assembly of distributary channels) in Figure 10b. However, it is unclear what mechanisms cause the observed downstream fining of bank material. One hypothesis is that there is a tendency for fining of suspended sediment downstream, such that coarser sediment is preferentially extracted to the banks and floodplain. For example, Lamb and Venditti (2016) suggested that downstream of gravel-sand transitions, rivers lose capacity to transport medium to coarse sand as wash load. Instead, sand is transported as bed material load (i.e., bed load and suspended bed material

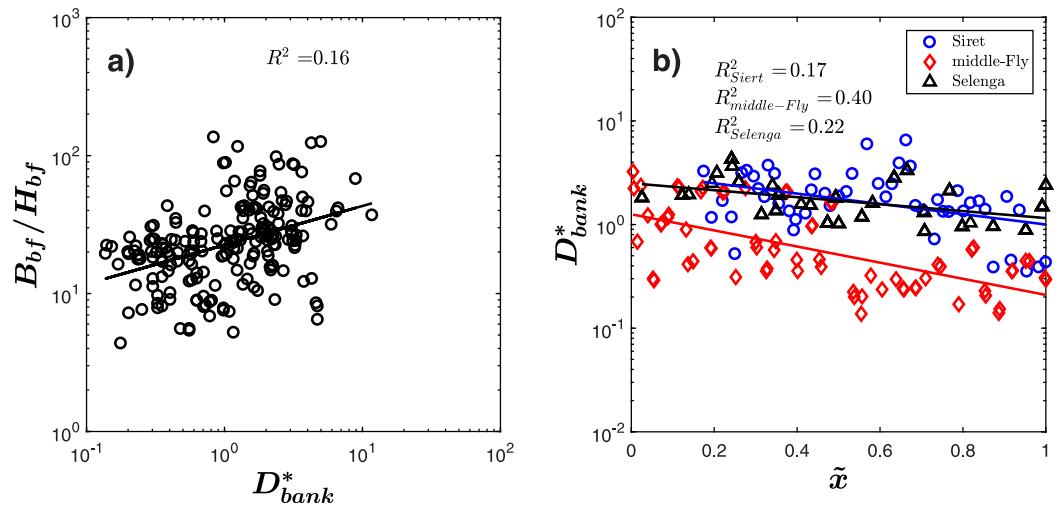


**Figure 10.** (a) Dimensionless bank sediment size as a power law function of width-depth ratio. (b) Downstream fining of dimensionless bank sediment size from the Selenga River delta, the middle Fly River, and the Siret River. Here  $\tilde{x}$  is normalized stream distance, equal to  $\tilde{x} = \frac{x}{x_{outlet}}$ ;  $x$  is distance downstream of a datum, and  $x_{outlet}$  is the total distance between the datum and river outlet.

load). Because channel banks are constructed by suspended material and wash load via overbank flow during flooding, downstream fining of bank material would be expected (Leopold et al., 1964).

### 5.3. Model Limitations

Results of the AIC test indicate that regression models obtained in this study perform better than the models generated via OLS from Li et al. (2016). This is because the orthogonal regression (major axis) used here considers error in the response variable. However, for the MA regression models, retention of bank sediment size in the bankfull Shields number and shear velocity relations does not drastically improve the model predictability, and the residuals remain unexplained (Table 4). A potential reason for this is that bank sediment size, although a good first-order approximation, does not fully characterize channel bank properties. Processes that govern bank strength may be poorly constrained by the treatments quoted above. As shown in section 5.2, for the most part, methods that describe physical processes of bank stability contain several empirically defined parameters, which are also difficult to measure. Moreover, bankfull shear velocity is nearly independent of both bank and bed sediment size. It is promising, however, that the bankfull depth relations including  $D_{bank}$  are superior in term of both absolute ( $R^2$ ) and relative (AIC value) predictive quality. This finding indicates that bank strength/properties do come into the picture of hydraulic geometry when bank grain size is included.

## 6. Conclusions

The main contribution of the present work is the quantification for the effect of characteristic bank material size on hydraulic geometry of rivers. Specifically, this study uses bank sediment grain size as a first parameterization for the role of bank material in setting formative (bankfull) channel Shields number. Key results from this study are as follows:

1. An empirical relation for bankfull Shields number as a function of slope, characteristic bed sediment grain size, and bank sediment grain size is computed, based on data from the distributary system of the delta of the Selenga River, Russia, the Middle Fly River, Papua New Guinea, the Siret River, Romania, the Llano River, Texas, and a set of English gravel rivers. This data base includes the relatively few instances in which systematic data on the downstream variation of bank grain size are available. The relation deriving from our work shows that bankfull Shields number is inversely related to bank sediment size.
2. Bankfull shear velocity and depth relations are derived based on the new empirical form of bankfull Shields number presented here. Both these parameters are found to be measurably dependent on bank sediment size.

3. The predictive relation for bankfull width for sand-bed streams obtained here is strongly dependent on bank sediment size and sediment discharge. This may be in part because coarser bank sediment can be easier to erode than fine bank sediment, which can be bound by cohesion and vegetation roots.
4. Sand-bed channels of the Selenga River delta have smaller Shields numbers than nondeltaic alluvial rivers.

Findings from this study show that to a first-order approximation, bank characteristics can be quantified in terms of a characteristic grain size in the computation of bankfull hydraulic geometry. It should be kept in mind, however, that there are many other factors that contribute to the ease of erosion or deposition of bank sediment, including friction angle, root cohesion, and subaerial vegetation establishment. We implicitly assume here that these factors correlate with bank grain size, but this may not universally be the case. Moreover, our analysis is empirical in nature; a full theory represents a future challenge, which we hope is motivated by our work.

#### Acknowledgments

We greatly appreciate Kevin Oberg from the United States Geological Survey (USGS) for calibrating and testing the Russian velocimeter at their Instrumentation Laboratory. The authors would like to thank Jan Pietron and Denis Aybulatov for providing field support, and Ni Yang for providing useful discussions about the statistical method. We also would like to thank Rob Ferguson and two anonymous reviewers for providing insightful comments and edits that significantly improved the quality of this manuscript. MATLAB script that performs the major axis regression, and spreadsheets that contain data of global rivers and Selenga River delta used in this study are available online under the supporting information. We thank Rice University for the partial financial support. This research was supported in part by National Science Foundation grant EAR-1415944. Russian group was additionally supported by Russian Fund for Basic Research Project 17-29-05027 (field work) and Russian Scientific Foundation 18-17-00086. The research work on which this manuscript is based was carried out in cooperation with the international research initiative Basenet (Baikal-Selenga Network).

#### References

- Aberle, J., Nikora, V., & Walters, R. (2004). Effects of bed material properties on cohesive sediment erosion. *Marine Geology*, 207(1–4), 83–93. <https://doi.org/10.1016/j.margeo.2004.03.012>
- Akaike, H. (1974). A new look at the statistical model identification. *IEEE Transactions on Automatic Control*, 19(6), 716–723. <https://doi.org/10.1109/TAC.1974.1100705>
- Andrews, E. D. (1984). Bed-material entrainment and hydraulic geometry of gravel-bed rivers in Colorado. *Geological Society of America Bulletin*, 95(3), 371–378. [https://doi.org/10.1130/0016-7606\(1984\)95<371:BEAHGO>2.0.CO;2](https://doi.org/10.1130/0016-7606(1984)95<371:BEAHGO>2.0.CO;2)
- Banks, H. T., & Joyner, M. L. (2017). AIC under the framework of least squares estimation. *Applied Mathematics Letters*, 74, 33–45. <https://doi.org/10.1016/j.aml.2017.05.005>
- Blom, A., Viparelli, E., & Chavarrías, V. (2016). The graded alluvial river: Profile concavity and downstream fining. *Geophysical Research Letters*, 43, 6285–6293. <https://doi.org/10.1002/2016GL068898>
- Bray, D. I. (1982). *Regime relations for gravel-bed rivers*, in *Gravel-Bed Rivers* (pp. 517–542). In Hey, R. D., Bathurst, J. C., & Thorne, C. R. (Eds.). Chichester, UK: John Wiley.
- Buffington, J. M., Dietrich, W. E., & Kirchner, J. W. (1992). Friction angle measurements on a naturally formed gravel streambed: Implications for critical boundary shear stress. *Water Resources Research*, 28(2), 411–425. <https://doi.org/10.1029/91WR02529>
- Burnham, K. P., & Anderson, D. R. (2004). Multimodel Inference. *Sociological Methods & Research*, 33(2), 261–304. <https://doi.org/10.1177/0049124104268644>
- Burnham, K. P., Anderson, D. R., & Huyvaert, K. P. (2011). AIC model selection and multimodel inference in behavioral ecology: Some background, observations, and comparisons. *Behavioral Ecology and Sociobiology*, 65(1), 23–35. <https://doi.org/10.1007/s00265-010-1029-6>
- Chalov, S., Thorslund, J., Kasimov, N., Aybulatov, D., Il'icheva, E., Karthe, D., et al. (2016). The Selenga River delta: A geochemical barrier protecting Lake Baikal waters. *Regional Environmental Change*, 17(7), 2039–2053. <https://doi.org/10.1007/s10113-016-0996-1>
- Coleman, S. M. (1998). Water-level changes in Lake Baikal, Siberia: Tectonism versus climate. *Geology*, 26(6), 531–534. [https://doi.org/10.1130/0091-7613\(1998\)026<0531:WLCLB>2.3.CO;2](https://doi.org/10.1130/0091-7613(1998)026<0531:WLCLB>2.3.CO;2)
- Cui, Y., & Parker, G. (1998). The arrested gravel front: Stable gravel-sand transitions in rivers. Part 2: General numerical solutions. *Journal of Hydraulic Research*, 36(2), 159–182. <https://doi.org/10.1080/00221689809498631>
- Czapiga, M. J., McElroy, B., & Parker, G. Bankfull shields number versus slope and grain size: Resolving a discrepancy. *Journal of Hydraulic Research*, <https://doi.org/10.1080/00221686.2018.1534287>
- Dade, W. B., & Friend, P. F. (1998). Grain-size, sediment-transport regime, and channel slope in alluvial rivers. *The Journal of Geology*, 106(6), 661–676. <https://doi.org/10.1086/516052>
- Dafalla, M. A. (2013). Effects of clay and moisture content on direct shear tests for clay-sand mixtures. *Advances in Materials Science and Engineering*, 2013, 562726. <https://doi.org/10.1155/2013/562726>
- Darby, S. E., & Thorne, C. R. (1996). Development and testing of riverbank-stability analysis. *Journal of Hydraulic Engineering*, 122(8), 443–454. [https://doi.org/10.1061/\(ASCE\)0733-9429\(1996\)122:8\(443\)](https://doi.org/10.1061/(ASCE)0733-9429(1996)122:8(443))
- Dietrich, W. E. (1982). Settling velocity of natural particles. *Water Resources Research*, 18(6), 1615–1626. <https://doi.org/10.1029/WR018i006p01615>
- Dietrich, W. E., Day, G., & Parker, G. (1999). The Fly River, Papua New Guinea: Inferences about river dynamics, floodplain sedimentation and fate of sediment. In A. J. Miller & A. Gupta (Eds.), *Varieties of fluvial form* (pp. 345–376). New York, NY: John Wiley & Sons.
- Dong, T. Y., Nittrouer, J. A., Il'icheva, E., Pavlov, M., McElroy, B., Czapiga, M. J., et al. (2016). Controls on gravel termination in seven distributary channels of the Selenga River delta, Baikal Rift basin, Russia. *Geological Society of America Bulletin*, 128(7–8), 1297–1312. <https://doi.org/10.1130/B31427.1>
- Eaton, B. C. (2006). Bank stability analysis for regime models of vegetated gravel bed rivers. *Earth Surface Processes and Landforms*, 31(11), 1438–1444. <https://doi.org/10.1002/esp.1364>
- Eaton, B. C., & Giles, T. R. (2009). Assessing the effect of vegetation-related bank strength on channel morphology and stability in gravel-bed streams using numerical models. *Earth Surface Processes and Landforms*, 34(5), 712–724. <https://doi.org/10.1002/esp.1768>
- Eaton, B. C., & Millar, R. G. (2004). Optimal alluvial channel width under a bank stability constraint. *Geomorphology*, 62(1), 35–45. <https://doi.org/10.1016/j.geomorph.2004.02.003>
- Eaton, B. C., & Millar, R. (2017). Predicting gravel bed river response to environmental change: The strengths and limitations of a regime-based approach. *Earth Surface Processes and Landforms*, 42(6), 994–1008. <https://doi.org/10.1002/esp.4058>
- Eke, E., Parker, G., & Shimizu, Y. (2014). Numerical modeling of erosional and depositional bank processes in migrating river bends with self-formed width: Morphodynamics of bar push and bank pull. *Journal of Geophysical Research: Earth Surface*, 119, 1455–1483. <https://doi.org/10.1002/2013JF003020>
- Engelund, F., & Hansen, E. (1967). *A monograph on sediment transport in alluvial streams*. Copenhagen, Denmark: TEKNISKFORLAG Skelbreggade 4.

- Foreman, B. Z., Heller, P. L., & Clementz, M. T. (2012). Fluvial response to abrupt global warming at the Palaeocene/Eocene boundary. *Nature*, *490*(7422), 92–95. <https://doi.org/10.1038/nature11513>
- Gabet, E. J. (1998). Lateral migration and bank erosion in a saltmarsh tidal channel in San Francisco Bay, California. *Estuaries and Coasts*, *21*(4), 745–753. <https://doi.org/10.2307/1353278>
- Galloway, W. E. (1975). Process framework for describing the morphologic and stratigraphic evolution of deltaic depositional systems. In M. L. Broussard (Ed.), *Deltas: models for exploration* (pp. 87–98). Houston, TX: Houston Geological Society.
- Garcia, M. H. (2008). *Sedimentation engineering: Processes, measurements, modeling and practice* (CE Manuals and Rep. on Eng. Practice 110). Reston, VA: American Society of Civil Engineers. ISBN: 978-0-7844-0814-8.
- Gilbert, G. K. (1885). *The topographic features of lake shores*. Washington, DC: U.S. Government Printing Office.
- Golub, G. H., & Van Loan, C. F. (1980). An analysis of the total least squares problem. *SIAM Journal on Numerical Analysis*, *17*(6), 883–893. <https://doi.org/10.1137/0717073>
- Gyninova, A. B., & Korsunov, V. M. (2006). The soil cover of the Selenga delta area in the Baikal region. *Eurasian Soil Science*, *39*(3), 243–250. <https://doi.org/10.1134/S1064229306030021>
- Hack, J. T. (1957). *Studies of longitudinal stream profiles in Virginia and Maryland* (Vol. 294). Washington, DC: U.S. Government Printing Office.
- Heiri, O., Lotter, A. F., & Lemcke, G. (2001). Loss on ignition as a method for estimating organic and carbonate content in sediments: Reproducibility and comparability of results. *Journal of Paleolimnology*, *25*(1), 101–110. <https://doi.org/10.1023/A:1008119611481>
- Heitmüller, F. T., & Hudson, P. F. (2009). Downstream trends in sediment size and composition of channel-bed, bar, and bank deposits related to hydrologic and lithologic controls in the Llano River watershed, central Texas, USA. *Geomorphology*, *112*(3), 246–260. <https://doi.org/10.1016/j.geomorph.2009.06.010>
- Hey, R. D., & Thorne, C. R. (1986). Stable channels with mobile gravel beds. *Journal of Hydraulic Engineering*, *112*(8), 671–689. [https://doi.org/10.1061/\(ASCE\)0733-9429\(1986\)112:8\(671\)](https://doi.org/10.1061/(ASCE)0733-9429(1986)112:8(671))
- Howard, A. D. (1992). Modeling channel migration and floodplain sedimentation in meandering streams. P. In Carling & G. E. Petts (Eds.), *Lowland floodplain rivers: Geomorphological perspectives* (pp. 1–41). Hoboken, NJ: John Wiley.
- Huang, Y. H. (1983). *Stability analysis of earth slopes*. New York, NY: Van Nostrand Reinhold.
- Hutchinson, D. R., Golmshtok, A. J., Zonenshain, L. P., Moore, T. C., Schloz, C. A., & Klitgord, K. D. (1992). Depositional and tectonic framework of the rift basins of Lake Baikal from multichannel seismic data. *Geology*, *20*(7), 589–592. [https://doi.org/10.1130/0091-7613\(1992\)020<0589:DATFOT>2.3.CO;2](https://doi.org/10.1130/0091-7613(1992)020<0589:DATFOT>2.3.CO;2)
- Ichim, I., & Radoane, M. (1990). Channel sediment variability along a river: A case study of the Siret River (Romania). *Earth Surface Processes and Landforms*, *15*(3), 211–225. <https://doi.org/10.1002/esp.3290150304>
- Il'icheva, E. A. (2008). Dynamics of the Selenga river network and delta structure. *Geography and Natural Resources*, *29*(4), 343–347. <https://doi.org/10.1016/j.gnr.2008.10.011>
- Il'icheva, E. A., Gagarinova, O. V., & Pavlov, M. V. (2015). Hydrologo-geomorphological analysis of landscape formation within the Selenga river delta. *Geography and Natural Resources*, *36*(3), 263–270. <https://doi.org/10.1134/S1875372815030063>
- Il'icheva, E. A., Pavlov, M. V., & Korytny, L. M. (2014). The river network of the Selenga delta at present. *Tomsk State University Journal*, *380*, 190–194. <https://doi.org/10.17223/15617793/380/32>
- Kellerhals, R., Bray, D. I., & Church, M. (1976). *Classification and analysis of river processes*. *Journal of the Hydraulics Division*, *102*(7), 813–829.
- Kirchner, J. W., Dietrich, W. E., Iseya, F., & Ikeda, H. (1990). The variability of critical shear stress, friction angle, and grain protrusion in water-worked sediments. *Sedimentology*, *37*(4), 647–672. <https://doi.org/10.1111/j.1365-3091.1990.tb00627.x>
- Krivonogov, S. K., & Safonova, I. Y. (2016). Basin structures and sediment accumulation in the Baikal Rift Zone: Implications for Cenozoic intracontinental processes in the Central Asian Orogenic Belt. *Gondwana Research*, *47*, 267–290. <https://doi.org/10.1016/j.gr.2016.11.009>
- Kulchitsky, A. S. (1964). Geological Map of the USSR. Scale 1:200 000 (Series Pribaikalskaya, Sheet N-48-XXXV) [in Russian]. Moscow: Nedra.
- Lane, E. W. (1955). *Importance of fluvial morphology in hydraulic engineering* (Vol. 81, paper no. 745). Reston, VA: American Society of Civil Engineers.
- Lamb, M. P., & Venditti, J. G. (2016). The grain size gap and abrupt gravel-sand transitions in rivers due to suspension fallout. *Geophysical Research Letters*, *43*, 3777–3785. <https://doi.org/10.1002/2016GL068713>
- Lane, E. W., Lin, P. N., & Liu, H. K. (1959). *The most efficient stable channel for completely clear water in non-cohesive material* (Colorado State Univ. Rep. CER 59 HKL 5). Fort Collins, CO: Colorado State University.
- Lee, J. S., & Julien, P. Y. (2006). Downstream hydraulic geometry of alluvial channels. *Journal of Hydraulic Engineering*, *132*(12), 1347–1352. [https://doi.org/10.1061/\(ASCE\)0733-9429\(2006\)132:12\(1347\)](https://doi.org/10.1061/(ASCE)0733-9429(2006)132:12(1347))
- Leopold, L. B., & Maddock, T. (1953). *The hydraulic geometry of stream channels and some physiographic implications* (U.S. Geol. Surv. Prof. Pap. 252, 57 p.). Washington, DC: U.S. Government Printing Office.
- Leopold, L. B., & Wolman, M. G. (1957). *River channel patterns: Braided, meandering and straight* (U.S. Geol. Surv. Prof. Pap. 282, pp. 39–85). Washington, DC: U.S. Government Printing Office.
- Leopold, L. B., Wolman, M. G., & Miller, J. P. (1964). *Fluvial processes in geomorphology* (522 pp.). London, UK: W. H. Freeman.
- Li, C., Czapiaga, M. J., Eke, E. C., Viparelli, E., & Parker, G. (2015). Variable Shields number model for river bankfull geometry: Bankfull shear velocity is viscosity-dependent but grain size-independent. *Journal of Hydraulic Research*, *53*(1), 36–48. <https://doi.org/10.1080/00221686.2014.939113>
- Li, C., Czapiaga, M. J., Eke, E. C., Viparelli, E., & Parker, G. (2016). Variable Shields number model for river bankfull geometry: Bankfull shear velocity is viscosity dependent but grain size-independent. *Journal of Hydraulic Research*, *54*(2), 234–237. <https://doi.org/10.1080/00221686.2015.1137088>
- Logatchev, N. A. (1974). Sayan-Baikal-Stanavoy upland. In *Uplands of the Pribaikalia and Zabaikalia* (pp. 16–162). Moscow, Russia: Nauka.
- Ma, H., Nittrouer, J. A., Naito, K., Fu, X., Zhang, Y., Moodie, A. J., et al. (2017). The exceptional sediment load of fine-grained dispersal systems: Example of the Yellow River, China. *Science Advances*, *3*(5), 1–8. <https://doi.org/10.1126/sciadv.1603114>
- Mackin, J. H. (1948). Concept of the graded river. *Geological Society of America Bulletin*, *59*(5), 463–512. [https://doi.org/10.1130/00167606\(1948\)59\[463:COTGR\]2.0.CO;2](https://doi.org/10.1130/00167606(1948)59[463:COTGR]2.0.CO;2)
- Markovsky, I., & Van Huffel, S. (2007). Overview of total least-squares methods. *Signal Processing*, *87*(10), 2283–2302. <https://doi.org/10.1016/j.sigpro.2007.04.004>
- Micheli, E. R., & Kirchner, J. W. (2002). Effects of wet meadow riparian vegetation on streambank erosion. 2: Measurements of vegetated bank strength and consequences for failure mechanics. *Earth Surface Processes and Landforms*, *27*(7), 687–697. <https://doi.org/10.1002/esp.340>
- Millar, R. G. (2005). Theoretical regime equations for mobile gravel-bed rivers with stable banks. *Geomorphology*, *64*(3–4), 207–220. <https://doi.org/10.1016/j.geomorph.2004.07.001>

- Millar, R. G., & Quick, M. C. (1993). Effect of bank stability on geometry of gravel rivers. *Journal of Hydraulic Engineering*, 119(12), 1343–1363. [https://doi.org/10.1061/\(ASCE\)0733-9429\(1995\)121:4\(382\)](https://doi.org/10.1061/(ASCE)0733-9429(1995)121:4(382))
- Muto, T., Furubayashi, R., Tomer, A., Sato, T., Kim, W., Naruse, H., et al. (2016). Planform evolution of deltas with graded alluvial topsets: Insights from three-dimensional tank experiments, geometric considerations and field applications. *Sedimentology*, 63(7), 2158–2189. <https://doi.org/10.1111/sed.12301>
- Parker, G. (1976). On the cause and characteristic scales of meandering and braiding in rivers. *Journal of Fluid Mechanics*, 76(3), 457–180. <https://doi.org/10.1017/S0022112076000748>
- Parker, G. (1978a). Self-formed straight rivers with equilibrium banks and mobile bed. Part 1: The sand-silt river. *Journal of Fluid Mechanics*, 89(1), 109–125. <https://doi.org/10.1017/S0022112078002499>
- Parker, G. (1978b). Self-formed straight rivers with equilibrium banks and mobile bed. Part 2: The gravel river. *Journal of Fluid Mechanics*, 89(1), 127–146. <https://doi.org/10.1017/S0022112078002505>
- Parker, G. (1991). Selective sorting and abrasion of river gravel. II: Applications. *Journal of Hydraulic Engineering*, 117(2), 150–171. [https://doi.org/10.1061/\(ASCE\)0733-9429\(1991\)117:2\(150\)](https://doi.org/10.1061/(ASCE)0733-9429(1991)117:2(150))
- Parker, G. (2004). *1D sediment transport morphodynamics with applications to rivers and turbidity currents* (E-book). Champaign, IL: University of Illinois. Retrieved from [http://hydrolab.illinois.edu/people/parkerg/morphodynamics\\_e-book.htm](http://hydrolab.illinois.edu/people/parkerg/morphodynamics_e-book.htm)
- Parker, G., & Cui, Y. (1998). The arrested gravel front: Stable gravel-sand transitions in rivers. Part 1: Simplified analytical solutions. *Journal of Hydraulic Research*, 36(1), 75–100. <https://doi.org/10.1080/00221689809498379>
- Parker, G., Muto, T., Akamatsu, Y., Dietrich, W. E., & Lauer, J. W. (2008). Unravelling the conundrum of river response to rising sea-level from laboratory to field. Part II. The Fly-Strickland River system, Papua New Guinea. *Sedimentology*, 55(6), 1657–1686. <https://doi.org/10.1111/j.1365-3091.2008.00962.x>
- Parker, G., Shimizu, Y., Wilkerson, G. V., Eke, E. C., Abad, J. D., Lauer, J. W., et al. (2011). A new framework for modeling the migration of meandering rivers. *Earth Surface Processes and Landforms*, 36(1), 70–86. <https://doi.org/10.1002/esp.2113>
- Parker, G., Toro-Escobar, C. M., Ramey, M., & Beck, S. (2003). Effect of floodwater extraction on mountain stream morphology. *Journal of Hydraulic Engineering*, 129(11), 885–895. [https://doi.org/10.1061/\(ASCE\)0733-9429\(2003\)129:11\(885\)](https://doi.org/10.1061/(ASCE)0733-9429(2003)129:11(885))
- Parker, G., Wilcock, P. R., Paola, C., Dietrich, W. E., & Pitlick, J. (2007). Physical basis for quasi-universal relations describing bankfull hydraulic geometry of single-thread gravel bed rivers. *Journal of Geophysical Research*, 112, F04005. <https://doi.org/10.1029/2006JF000549>
- Pfeiffer, A. M., Finnegan, N. J., & Willenbring, J. K. (2017). Sediment supply controls equilibrium channel geometry in gravel rivers. *Proceedings of the National Academy of Sciences of the United States of America*, 114(13), 3346–3351. <https://doi.org/10.1073/pnas.1612907114>
- Phillips, C. B., & Jerolmack, D. J. (2016). Self-organization of river channels as a critical filter on climate signals. *Science*, 352(6286), 694–697. <https://doi.org/10.1126/science.aad3348>
- Scholz, C. A., Moore, T. C., Hutchinson, D. R., Ja Golmshtok, A., Klitgord, K. D., & Kurotchkin, A. G. (1998). Comparative sequence stratigraphy of low-latitude versus high-latitude lacustrine rift basins: Seismic data examples from the East African and Baikal rifts. *Palaeogeography Palaeoclimatology Palaeoecology*, 140(1–4), 401–420. [https://doi.org/10.1016/S0031-0182\(98\)00022-4](https://doi.org/10.1016/S0031-0182(98)00022-4)
- Shields, A. (1936). *Application of similarity principles and turbulence research to bed-load movement*. Pasadena, CA: Soil Conservation Service Cooperative Laboratory, California Institute of Technology.
- Singh, V. P. (2003). On the theories of hydraulic geometry. *International Journal of Sediment Research*, 18(3), 196–218.
- Simon, A., & Collison, A. J. (2002). Quantifying the mechanical and hydrologic effects of riparian vegetation on streambank stability. *Earth Surface Processes and Landforms*, 27(5), 527–546. <https://doi.org/10.1002/esp.325>
- Simon, A., Curini, A., Darby, S. E., & Langendoen, E. J. (1999). *Streambank mechanics and the role of bank and near-bank processes in incised channels* (pp. 193–217). Chichester, UK: John Wiley & Sons.
- Simon, A., Curini, A., Darby, S. E., & Langendoen, E. J. (2000). Bank and near-bank processes in an incised channel. *Geomorphology*, 35(3), 193–217. [https://doi.org/10.1016/S0169-555X\(00\)00036-2](https://doi.org/10.1016/S0169-555X(00)00036-2)
- Simon, A., Wolfe, W. J., & Molinas, A. (1991). Mass wasting algorithms in an alluvial channel model. In Fan, S.-S., & Kuo, Y.-H. (Eds.), *Proceedings of the 5th federal inter-agency sedimentation conference* (pp. 22–29). Washington, DC: Federal Energy Regulatory Commission.
- Simons, D. B., & Albertson, M. L. (1960). Uniform water conveyance channels in alluvial materials. *Journal of the Hydraulics Division*, 86(5), 33–71.
- Smith, C. E. (1998). Modeling high sinuosity meanders in a small flume. *Geomorphology*, 25(1), 19–30. [https://doi.org/10.1016/S0169-555X\(98\)00029-4](https://doi.org/10.1016/S0169-555X(98)00029-4)
- Trampush, S. M., Huzurbazar, S., & McElroy, B. (2014). Empirical assessment of theory for bankfull characteristics of alluvial channels. *Water Resources Research*, 50, 9211–9220. <https://doi.org/10.1002/2014WR015597>
- Van Huffel, S. (1989). Analysis and properties of the generalized total least. *SIAM Journal of Numerical Analysis*, 10(3), 294–315.
- Van Rijn, L. C. (1984). Sediment transport. Part I: Bed load transport. *Journal of Hydraulic Engineering*, 110(10), 1431–1456. [https://doi.org/10.1061/\(ASCE\)0733-9429\(1984\)110:10\(1431\)](https://doi.org/10.1061/(ASCE)0733-9429(1984)110:10(1431))
- Wiberg, P. L., & Smith, J. D. (1987). Calculations of the critical shear stress for motion of uniform and heterogeneous sediments. *Water Resources Research*, 23(8), 1471–1480. <https://doi.org/10.1029/WR023i008p01471>
- Wilkerson, G. V., & Parker, G. (2011). Physical basis for quasi-universal relationships describing bankfull hydraulic geometry of sand-bed rivers. *Journal of Hydraulic Engineering*, 137(7), 739–753. [https://doi.org/10.1061/\(ASCE\)HY.1943-7900.0000352](https://doi.org/10.1061/(ASCE)HY.1943-7900.0000352)
- Williams, G. P. (1978). Bank-full discharge of rivers. *Water Resources Research*, 14(6), 1141–1154. <https://doi.org/10.1029/WR014i006p01141>
- Wu, T. H., McKinnell Iii, W. P., & Swanston, D. N. (1979). Strength of tree roots and landslides on Prince of Wales Island, Alaska. *Canadian Geotechnical Journal*, 16(1), 19–33. <https://doi.org/10.1139/t79-003>